



Since January 2020 Elsevier has created a COVID-19 resource centre with free information in English and Mandarin on the novel coronavirus COVID-19. The COVID-19 resource centre is hosted on Elsevier Connect, the company's public news and information website.

Elsevier hereby grants permission to make all its COVID-19-related research that is available on the COVID-19 resource centre - including this research content - immediately available in PubMed Central and other publicly funded repositories, such as the WHO COVID database with rights for unrestricted research re-use and analyses in any form or by any means with acknowledgement of the original source. These permissions are granted for free by Elsevier for as long as the COVID-19 resource centre remains active.



Review article

The development of Coronavirus 3C-Like protease ($3CL^{pro}$) inhibitors from 2010 to 2020

Yuzhi Liu ^a, Chengyuan Liang ^{a,*}, Liang Xin ^a, Xiaodong Ren ^b, Lei Tian ^a, Xingke Ju ^a, Han Li ^a, Yongbo Wang ^a, Qianqian Zhao ^a, Hong Liu ^{c, **}, Wenqiang Cao ^c, Xiaolin Xie ^d, Dezhu Zhang ^d, Yu Wang ^d, Yanlin Jian ^{e, ***}

^a Faculty of Pharmacy, Shaanxi University of Science & Technology, Xi'an, 710021, PR China

^b Medical College, Guizhou University, Guiyang, 550025, PR China

^c Zuhai Jinan Selenium Source Nanotechnology Co., Ltd., Hengqin, Zhuhai, Guangdong, 519030, PR China

^d Shaanxi Panlong Pharmaceutical Group Co., Ltd., Xi'an, 710025, PR China

^e Laboratory for Medicinal Chemistry (FFW), Ghent University, Ottergemsesteenweg 460, B9000, Gent, Belgium

ARTICLE INFO

Article history:

Received 22 June 2020

Received in revised form

17 July 2020

Accepted 29 July 2020

Available online 6 August 2020

Keywords:

Coronaviruses

3C-like protease ($3CL^{pro}$) inhibitors

Peptidomimetic inhibitors

COVID-19

Proteolytic targeting chimaera (PROTAC)

ABSTRACT

This review fully describes the coronavirus $3CL^{pro}$ peptidomimetic inhibitors and nonpeptidic small molecule inhibitors developed from 2010 to 2020. Specifically, the structural characteristics, binding modes and SARs of these $3CL^{pro}$ inhibitors are expounded in detail by division into two categories: peptidomimetic inhibitors mainly utilize electrophilic warhead groups to covalently bind the $3CL^{pro}$ Cys145 residue and thereby achieve irreversible inhibition effects, whereas nonpeptidic small molecule inhibitors mainly interact with residues in the S1', S1, S2 and S4 pockets via hydrogen bonds, hydrophobic bonds and van der Waals forces. Based on the emerging PROTAC technology and the existing $3CL^{pro}$ inhibitors, $3CL^{pro}$ PROTAC degraders are hypothesised to be next-generation anti-coronavirus drugs.

© 2020 Elsevier Masson SAS. All rights reserved.

Contents

1. Introduction	2
1.1. COVID-19 pandemic	2
1.2. Coronavirus and SARS-CoV-2	2
2. $3CL$ protease	3
3. Peptidomimetic $3CL^{pro}$ inhibitors	3
4. Nonpeptidic $3CL^{pro}$ inhibitor	5
4.1. Decahydroisoquinoline and octahydro-isochromene derivatives	5
4.2. $3CL^{pro}$ inhibitor with a 3-pyridyl or triazole moiety	6
4.3. $3CL^{pro}$ inhibitor with a piperidine moiety	8
4.4. Unsymmetrical aromatic disulphides	9
4.5. Serine derivatives	9
4.6. Pyrazolone and pyrimidines	9
4.7. Natural product derivatives	11
4.7.1. Flavonoids, biflavonoids and chalcones	11
4.7.2. Isatin derivatives	12

* Corresponding author.

** Corresponding author.

*** Corresponding author.

E-mail addresses: chengyuanliang@gmail.com (C. Liang), sesource_liuhong@163.com (H. Liu), yanlin.jian@ugent.be (Y. Jian).

4.7.3. Terpenoid derivatives	13
5. Discussion and perspectives	13
Declaration of competing interest	16
Acknowledgements	16
References	16

Abbreviation index

ACE2	Angiotensin-converting enzyme 2
3CL ^{pro}	3C-like Protease
E	Envelope protein
EUA	Emergency use authorization
FDA	The U.S. Food and Drug Administration
GCG	Gallocatechin gallate
HCV	Hepatitis C virus
His-al	(S)-2-amino-3-imidazolyl propanal
HIV	Human immunodeficiency virus
HCoV	human coronavirus
M	Membrane protein
MERS-CoV	Middle East respiratory syndrome coronavirus
MLPCN	Molecular Libraries Probe Production Centers Network
M ^{pro}	Main protease

N	Nucleocapsid phosphoprotein
NA	Neuraminidase
NIH	National Institutes of Health
nsps	Non-structural proteins
ORF	Open reading frames
PL ^{pro}	Papain-like protease
PK	pharmacokinetic
PROTAC	Proteolysis-targeting chimaera
QD	Once a day
RdRp	RNA-dependent RNA polymerase
S	Spike protein
SAR	Structure-activity relationship
SARS-CoV	Severe acute respiratory syndrome coronavirus
SARS-CoV-2	Severe acute respiratory syndrome coronavirus 2
SFC	Supercritical fluid chromatography
SPR	Surface plasmon resonance

1. Introduction

1.1. COVID-19 pandemic

Coronavirus disease 2019 (COVID-19) is a highly infectious disease caused by severe acute respiratory syndrome coronavirus 2 (SARS-CoV-2), a virus that is closely related to the SARS virus [1]. On May 15, 2020, the COVID-19 pandemic had spread to 210 countries, and more than 4.5 million people had been diagnosed with the infection worldwide [2,3]. SARS-CoV-2 primarily spreads by small droplets expelled by infected individuals when they breathe or cough [4,5]. The infected individuals may either be asymptomatic or develop common COVID-19 symptoms, including fever, cough, fatigue, shortness of breath, and loss of smell [6], and severe cases can progress to complications, including pneumonia, acute respiratory distress syndrome, multi-organ failure, and death [7]. The fatality rate is estimated to be between 3% and 6%. There is no vaccine or specific antiviral treatment for COVID-19, and the available treatments involve symptom management, supportive care, and experimental alternative medicines.

1.2. Coronavirus and SARS-CoV-2

Coronaviruses are species of viruses belonging to the subfamily *Orthocoronavirinae* in the family *Coronaviridae* of the order *Nidovirales*. Coronavirus is a forward single-stranded RNA [8,9], which is endowed with the largest viral genomes (27–32 kb) among the RNA viruses identified to date [10]. Genomic RNA complexes with the basic nucleocapsid protein (N) to form a helical capsid within the membrane. The membrane of all coronaviruses is composed of a minimum of three viral proteins: (a) a spike protein (S), which is a type of glycoprotein I [11]; (b) a membrane protein (M) that spans the membrane; and c) an envelope protein (E) [12,13], which is a highly hydrophobic protein that covers the entire coronavirus

[14,15]. For a long time, coronaviruses have been recognized as important pathogens that cause respiratory and gastrointestinal diseases in birds and mammals. Before SARS-CoV-2, six coronaviruses had been found to infect humans: HCoV-229E, HCoV-OC43, HCoV-NL63, HCoV-HKU1, severe acute respiratory syndrome coronavirus (SARS-CoV) and Middle East respiratory virus coronavirus (MERS-CoV). The first four are constraint endemic strains that cause the common cold, whereas the latter two can cause serious respiratory epidemics [16–18]. SARS is an atypical viral respiratory disease that resulted in 8098 cases and 774 reported deaths in 17 countries (9.6% fatality rate) during a large-scale outbreak in 2003 [19–21]. Fortunately, the SARS epidemic was successfully contained under joint efforts. MERS is a zoonotic respiratory infection that initially broke out in the Middle East in 2012. According to the World Health Organization records, MERS coronavirus has thus far resulted in 2494 cases of infection and 858 deaths. Based on the high prevalence and widespread distribution of coronaviruses, as well as their genetic diversity and the frequent recombination of the genome, coronaviruses pose a continuous threat to humans [22–24].

Due to the current public health emergency due to COVID-19, the U.S. Food and Drug Administration (FDA) has issued an emergency use authorization (EUA) of the experimental drug remdesivir [25,26]. However, the efficacy and safety of remdesivir remain controversial. The Japanese Ministry of Health, Labour and Welfare has also approved remdesivir as a treatment for COVID-19. In addition, the combination of α -interferon and the anti-human immunodeficiency virus (HIV) drug lopinavir/ritonavir (Kaletra[®]) has been used to treat COVID-19, but the evidence regarding its effectiveness remains still limited, and the drug might have toxic side effects [26–28]. Therefore, the development of highly specific and effective anti-coronavirus drugs against key viral targets, particularly SARS-CoV-2, is urgently needed and would also be of great significance for preventing and treating the recurrence of coronavirus epidemics in the future.

2. 3CL protease

The coronavirus genome has a structure with a 5'-cap and a 3'-poly-A tail and contains 6–12 open reading frames (ORFs). The first ORF (ORF 1a/b) accounts for approximately two-thirds of the genome length and can directly translate two polyproteins, pp1a and pp1ab, according to an a-1 frameshift between ORF1a and ORF1b [29,30]. The abovementioned polyproteins are then incised and functionalized into 16 non-structural proteins (nsps) by 3CL protease ($3CL^{pro}$), which is also known as M^{pro} or papain-like protease (PLP) (Fig. 1) [31,32]. The coronavirus $3CL^{pro}$ is a cysteine protease composed of approximately 300 amino acids and contains three domains [33,34]. Active $3CL^{pro}$ is a homodimer that contains two promoters [35,36]. $3CL^{pro}$, which has a non-classical Cys-His catalytic dyad (Cys145 and His41) in the gap between domains I and II [37], can specifically recognize the 11 cleavage sites of nsp4–nsp16 and exhibits self-hydrolytic cleavage activity [12,38]. These functional nsp4–nsp16 released by cleavage with $3CL^{pro}$ are responsible for viral genome replication and transcription, and nsp4–nsp16 also play roles in other important viral life processes, such as protein translation, cleavage, and modification and nucleic acid synthesis [34,39]. Therefore, the inhibition of $3CL^{pro}$ can effectively block viral RNA replication and transcription and further block viral proliferation.

$3CL^{pro}$ is highly conserved among the known coronavirus species, and several common features are shared among the different coronavirus $3CL^{pro}$ substrates. From the N to the C terminus, the amino acids in the substrates are numbered as -P4-P3-P2-P1↓P1'-P2'-P3'-, and the cleavage site is located between P1 and P1' [40,41]. In particular, a Gln residue is almost always required in the P1 position of the substrates. Humans do not have a homologous $3CL^{pro}$, which makes $3CL^{pro}$ an ideal specific antiviral target. SARS-CoV-2 and SARS-CoV are significantly different from MERS-CoV in terms of cell invasion characteristics (the S protein of MERS-CoV utilizes DPP4 as a receptor). Nevertheless, amino acid sequence alignments indicate that the similarity of the $3CL^{pro}$ s of SARS-CoV-2, SARS-CoV and MERS-CoV can be as high as 96.1% [42,43]. Further sequence comparisons have revealed that the $3CL^{pro}$ s of the three coronaviruses of SARS-CoV-2, SARS-CoV, and MERS-CoV exhibits a high degree of structural similarity and conservatism (Fig. 2) [44]. These findings indicate that $3CL^{pro}$ could be used as a homologous target for the development of anti-coronavirus drugs that can inhibit the proliferation of various coronaviruses.

3. Peptidomimetic $3CL^{pro}$ inhibitors

Structurally, $3CL^{pro}$ inhibitors can be classified as peptoids and non-peptidomimetics, and the mechanism of action of peptide inhibitors includes two steps. Peptidomimetics that mimic natural peptide substrates initially bind to $3CL^{pro}$ and form a noncovalent complex, and the warhead group, which is spatially very close to the catalytic residue of the target protein, undergoes a nucleophilic

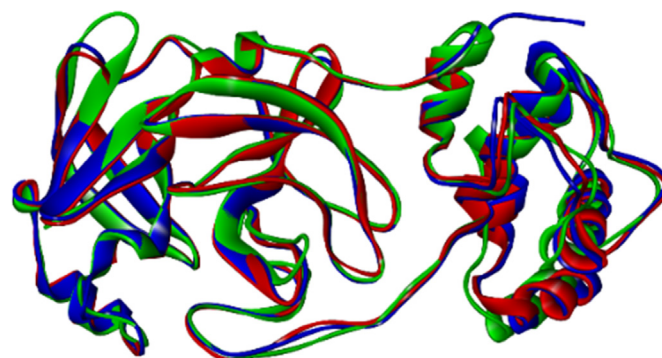


Fig. 2. Simulated superposition of the structures of SARS-CoV-2 $3CL^{pro}$ (PDB code: 6LU7, blue), SARS-CoV $3CL^{pro}$ (PDB code: 1Q2W, red), and MERS-CoV $3CL^{pro}$ (PDB code: 4RSP, green). (For interpretation of the references to colour in this figure legend, the reader is referred to the Web version of this article.)

attack to catalyse the formation of cysteine-participating covalent bonds [45,46]. These warheads mainly contain Michael receptors [47,48], aldehydes [49] and different types of ketones (see Fig. 3 and Table 1) [50–52], which covalently bind to the Cys145 residue in the $3CL^{pro}$ S1' pocket to exert an inhibitory effect.

Among these peptidomimetic inhibitors, the aldehyde compounds **11** and **12** and the α -ketoamide compounds **25–27** showed good inhibitory activity against the current SARS-CoV-2. Compounds **11** and **12**, which as novel inhibitors designed and synthesized for SARS-CoV-2 $3CL^{pro}$ by Hong Liu and his colleagues [62], demonstrate excellent inhibitory activity against SARS-CoV-2 $3CL^{pro}$ (**11**: $IC_{50} = 0.053 \pm 0.005 \mu\text{M}$, **12**: $IC_{50} = 0.040 \pm 0.002 \mu\text{M}$). Moreover, *in vitro* antiviral activity assays have indicated that both compounds exert potent anti-SARS-CoV-2 effects, with EC_{50} values of 0.53 μM and 0.72 μM , respectively, and both **11** and **12** exhibit good *in vivo* pharmacokinetic properties and an acceptable preliminary safety profile and have the potential to be new anti-SARS-CoV-2 preclinical candidates. Based on an analysis of the substrate binding pocket of SARS-CoV $3CL^{pro}$ (PDB CODE: 2H2Z), an aldehyde was selected as the warhead in P1 that would form a covalent bond with cysteine. A detailed diagram of the interaction between compound **11** and SARS-CoV-2 $3CL^{pro}$ shows that the aldehyde carbonyl of **11** and the catalytic site Cys145 of SARS-CoV-2 $3CL^{pro}$ form a standard C–S covalent bond (Fig. 4-A). The oxygen atom of the aldehyde group forms a hydrogen bond with the backbone of the Cys145 residue at the S1' site, which is crucial for stabilizing the binding conformation. The (S)- γ -lactam ring at P1 is in good agreement with the S1 site, and the oxygen atom of the (S)- γ -lactam group forms a hydrogen bond with the His163 side chain, the main chain of Phe140 and the side chain of Glu166 and also forms a hydrogen bond with the NH group of the (S)- γ -lactam ring. The cyclohexyl part at the P2 position can be inserted into the S2 position and stacks with the imidazole ring of His41. The indole group at the P3 position is exposed to the solvent (S4 site) and forms a hydrogen bond with Glu166. Interestingly, multiple water molecules (named W1–W6) play important roles in the binding of **11**: W1 interacts with the amide bond of **11** through hydrogen bonding, whereas W2–W6 form a few hydrogen bonds with the aldehyde group of **11** and the residues Asn142, Gly143, Thr26, Thr25, His41 and Cys44, which contribute to the stability of the binding pocket of **11**. The binding mode of compound **12** is very similar to that of **11** (Fig. 4-B). The difference in their binding modes might be due to the 3-fluorophenyl at the P2 position of compound **12**. The side chains of the residues His41, Met49, Met165, Val186, Asp187 and Arg188 interact with the aryl group through hydrophobic interactions, and the side chain of Gln189 stabilizes 3-fluorophenyl via additional hydrogen bonding.

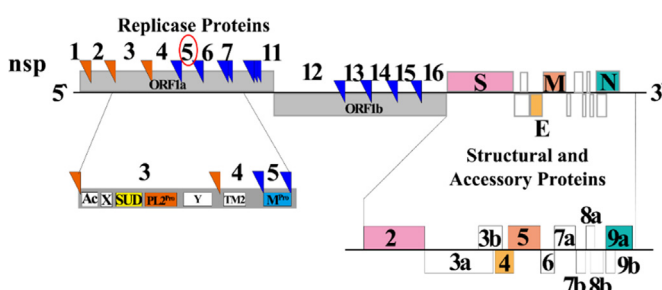


Fig. 1. Coronavirus (SARS-CoV) genome.

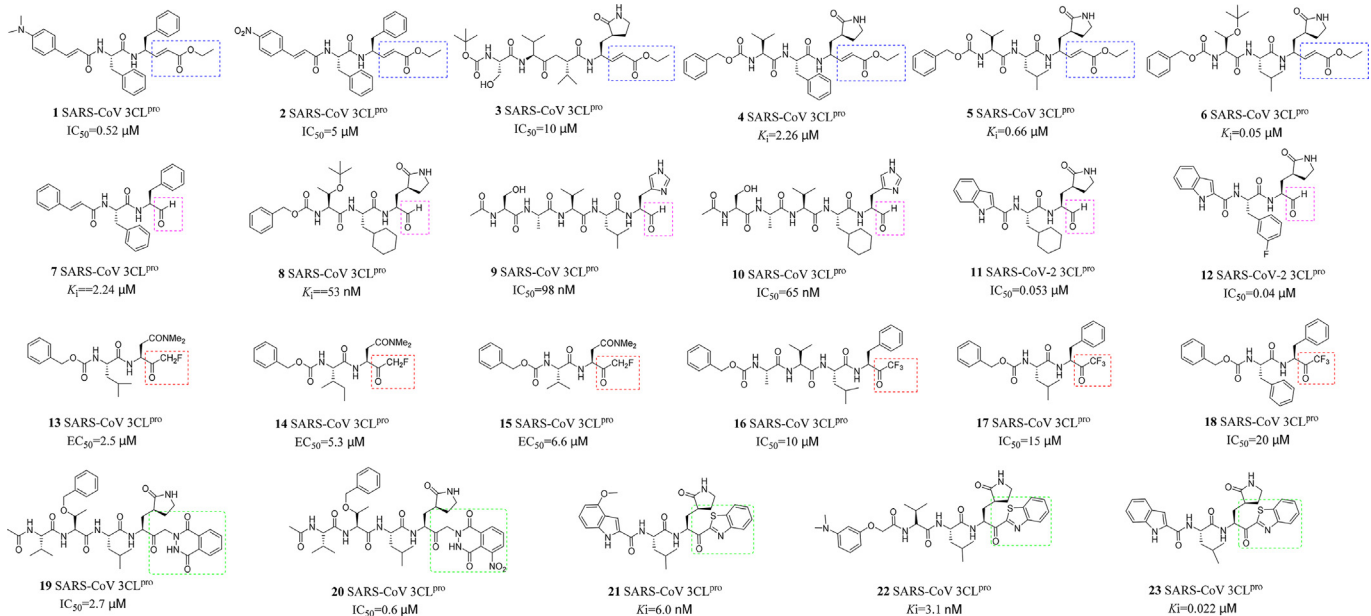


Fig. 3. Peptidomimetic 3CL^{pro} inhibitors.

Table 1
Peptidomimetic 3CL^{pro} inhibitors.

Type	Categories	Compound No.	Ref
1	Michael acceptor peptidomimetics	1–6	[53–55]
2	Aldehyde peptidomimetics	7–12	[55,56]
3	Keto peptidomimetics	13–27	[51]
3–1	Fluoromethyl ketone	13–18	[57]
3–2	1,4-Phthalazinedione	19–21	[58]
3–3	Benzothiazolone	22–23	[59,60]
3–4	α -Ketoamide	24–27	[61]

Rolf Hilgenfeld et al. previously revealed that the peptidomimetic α -ketoamide inhibitor **24** serves as a broad-spectrum inhibitor of the 3CL^{pro}s of β -coronaviruses, α -coronaviruses and enteroviruses [61]. Compound **24** exhibits a low EC₅₀ for SARS-CoV and a number of enteroviruses in different cell lines (EC₅₀ < 5 μ M); notably, the EC₅₀ of MERS-CoV in Huh7 cells is 400 pM. The lead **24** has been subjected to various structural modifications [63]. To improve its half-life in plasma, compound **24** was modified by hiding the P3–P2 amide bond on the pyridone ring (Fig. 5, green circle), which is expected to prevent off-target contacts and the

cleavage of this bond by other cellular proteases. In addition, to enhance the solubility of **24** in plasma, the hydrophobic cinnamyl was replaced by a low-hydrophobic Boc group (Fig. 5, red circle), which produced **25**. Moreover, the cyclohexyl at P2 of **25** was substituted for the smaller cyclopropyl (Fig. 5, blue circle) to render **26**, which might show enhanced antiviral activity against the β -coronaviruses of clade b (SARS-CoV-2 and SARS-CoV). However, compound **27**, which was obtained by removal of the Boc group of **26**, was almost inactive (Fig. 5, purple circle), which indicated that the hydrophobic group is necessary for crossing the cell membrane and binding to viral 3CL^{pro}. A pharmacokinetics study demonstrated that 4 h after its subcutaneous administration, the lung tissue concentration of **26** is approximately 13 ng/g. The lung tropism of **26** was a favourable target organ aggregation characteristic because COVID-19 and other coronaviruses mostly affect lung tissue. As a complementary route of administration, **26** can also be nebulized with an inhalation device at 3 mg/kg. Even 24 h after its administration, the concentration of **26** in lung tissue remains at 33 ng/g. A mouse lung drug inhalation model showed that **26** is well tolerated without adverse reactions, which indicates that inhalers might be a suitable method for the administration of **26**.

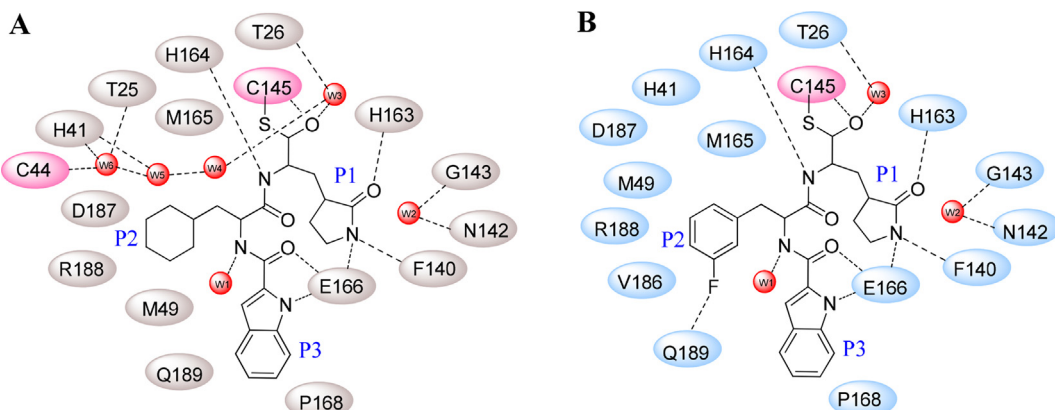


Fig. 4. Schematic diagram of the X-ray crystal structure: the interaction of compounds 11 (A) and 12 (B) with SARS-CoV-2 3CL^{pro}.

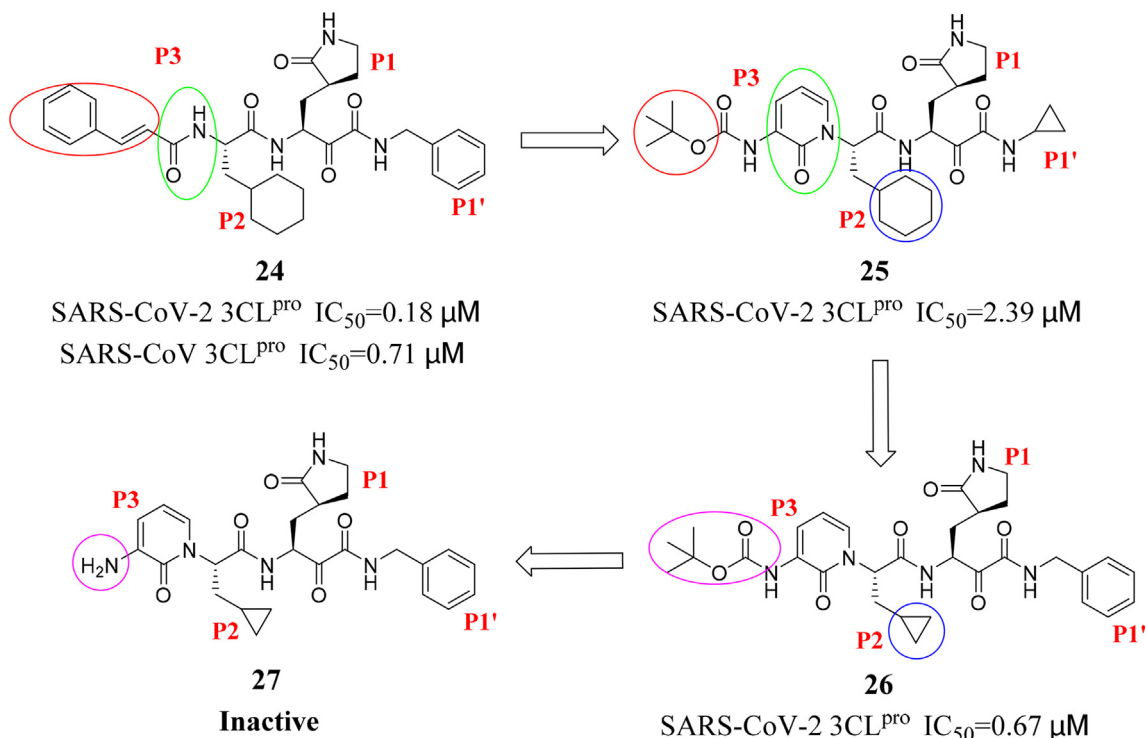


Fig. 5. Chemical structures of α -ketoamide inhibitors **24–26**. The coloured circles highlight the specific modifications during each development step.

The other peptidomimetic inhibitors shown in Fig. 3 and Table 1 were described in detail in a previous review by Thanigaimalai Pillaiyar et al. [64].

4. Nonpeptidic 3CL^{pro} inhibitor

4.1. Decahydroisoquinoline and octahydro-isochromene derivatives

Inspired by the interaction of the peptide inhibitor **28** between S1 and S2 of SARS-CoV 3CL^{pro} , Shimamoto Yasuhiro et al. [65] designed and synthesized a series of competitive SARS-CoV 3CL^{pro} inhibitors (compounds **29a–29d**, Fig. 6) with a decahydroisoquinoline fused

ring scaffold. All synthetic decahydroquinoline inhibitors exhibited moderate to significant inhibition of SARS 3CL^{pro} . According to X-ray crystallography (PDB CODE: 4TWY, Fig. 7), the fused ring structure of dehydroisoquinoline occupies most of the space in the S2 pocket. X-ray crystallography analyses have confirmed that the decahydroisoquinoline inhibitor is located in the fissure of the active centre of 3CL^{pro} , similar to the results obtained with the high-efficiency peptide-aldehyde lead compound. The decahydroisoquinoline scaffold was inserted into a large S2 pocket and filled most of the pocket space. As expected, the imidazole at the P1 site was inserted into the S1 pocket. These interactions effectively fixed the terminal aldehyde in the fissure of the active centre, and the new scaffold thus closely fit

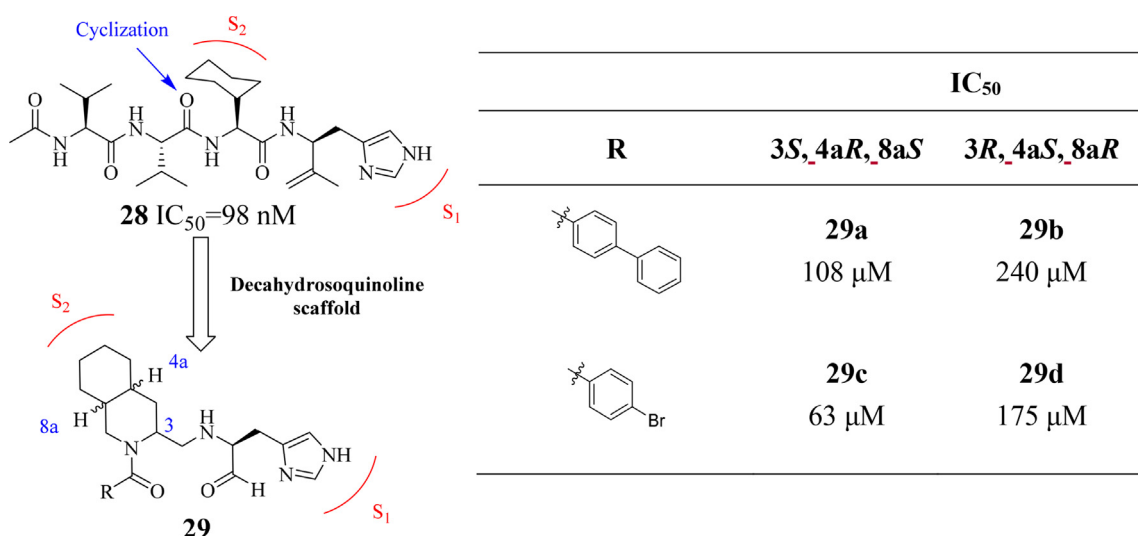


Fig. 6. Novel decahydroisoquinoline derivatives that serve as SARS-CoV 3CL^{pro} inhibitors.

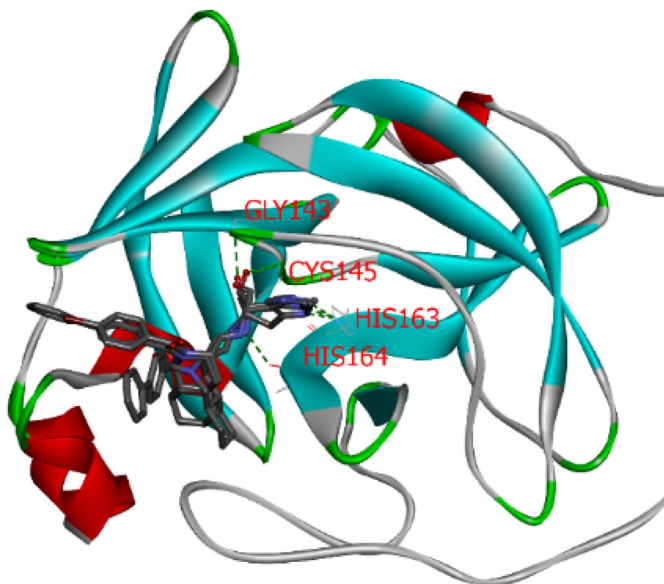


Fig. 7. Crystal structure of SARS-CoV 3CL^{pro} superimposed with **29a**, **29b** and **29c** (PDB code: 4TWY).

to the 3CL^{pro}. Acyl groups on nitrogen atoms in dehydroisoquinoline scaffolds are located on the surface of 3CL^{pro}, where additional interactions might occur with 3CL^{pro}. These interactions effectively fixed the terminal aldehyde tightly at the active site, resulting in a novel dehydroisoquinoline scaffold that cooperates closely with 3CL^{pro}. To evaluate the effect of the configuration on the dehydroisoquinoline scaffold, the IC₅₀ values of trans-dehydroisoquinolin diastereomers in N-4-phenylbenzoyl derivatives (**29a** vs **29b**) or N-4-bromo benzoyl derivatives (**29c** vs **29d**)

have been compared, and the results clearly showed that the (4aR,8aS) isomer is more potent than the (4aS,8aR) isomer.

Based on the abovementioned findings, Shimamoto Yasuhiro et al. performed further structural modifications, and an octahydro-isochromene scaffold was selected as a new type of hydrophobic fused ring (Fig. 8). An alkyl or aryl substituent was also introduced to the 1-position of the octahydro-isochromene scaffold. The effects of the configuration of the fused ring structure and those of various substituents on the inhibition of SARS 3CL^{pro} were evaluated. Sharpless-Katsuki asymmetric epoxidation and Sharpless asymmetric dihydroxylation were employed to synthesise the octahydro-isochromene moiety. Introduction of (S)-2-amino-3-imidazolyl propanal (His-al) at the P1 site and the substituent at the 1-position was achieved through successive reductive amination reactions. N-butyl (**30**), isobutyl (**31**), allyl (**32**) and benzyl (**33**) were introduced at the 1-position, and the IC₅₀ value for SARS 3CL^{pro} indicates that the n-butyl substituent is expected to form a certain interaction with the protease. The stereochemical effect of the octahydro-isochromene scaffold was also investigated, and the results showed that the specific (1S, 3S) configuration of **35** can orient imidazole and the warhead aldehyde at the P1 site to the corresponding 3CL^{pro} pockets [66] (see Fig. 9).

Additionally, Kouji Ohnishi et al. [67] introduced a non-prime site substituent at the 4-position carbon of the decahydroisoquinolin skeleton to yield the nonpeptidic inhibitor **38**, which exhibits moderate but enhanced inhibitory activity against R188I SARS 3CL^{pro} (IC₅₀ = 26 μM). The results indicated significantly increased affinity between **38** and SARS 3CL^{pro} at the S3 to S4 pockets.

4.2. 3CL^{pro} inhibitor with a 3-pyridyl or triazole moiety

Jacobs et al. [46] conducted a high-throughput screening of National Institute of Health (NIH) molecular libraries

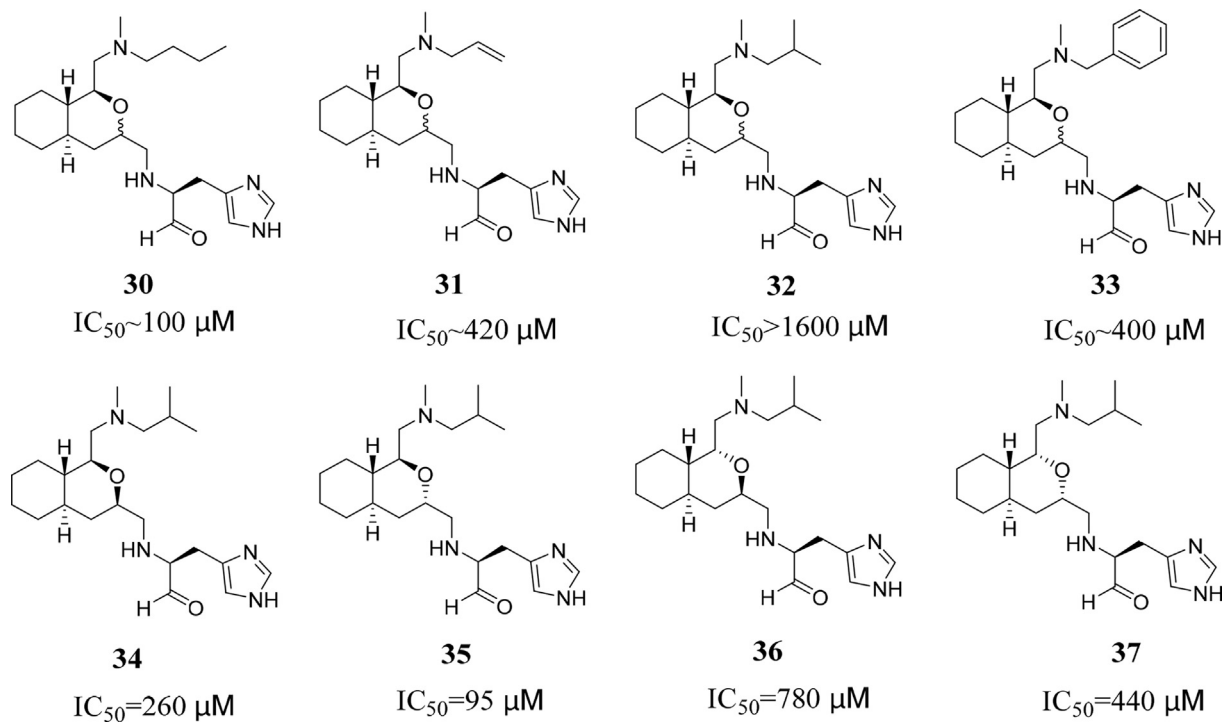
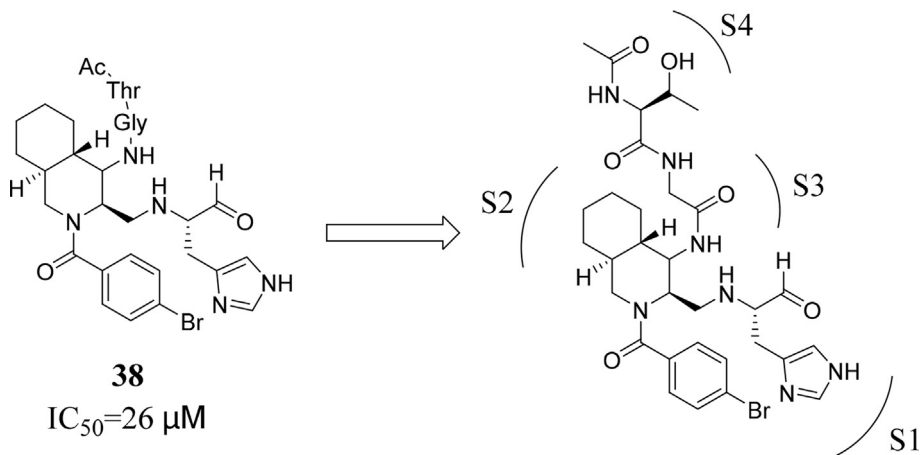
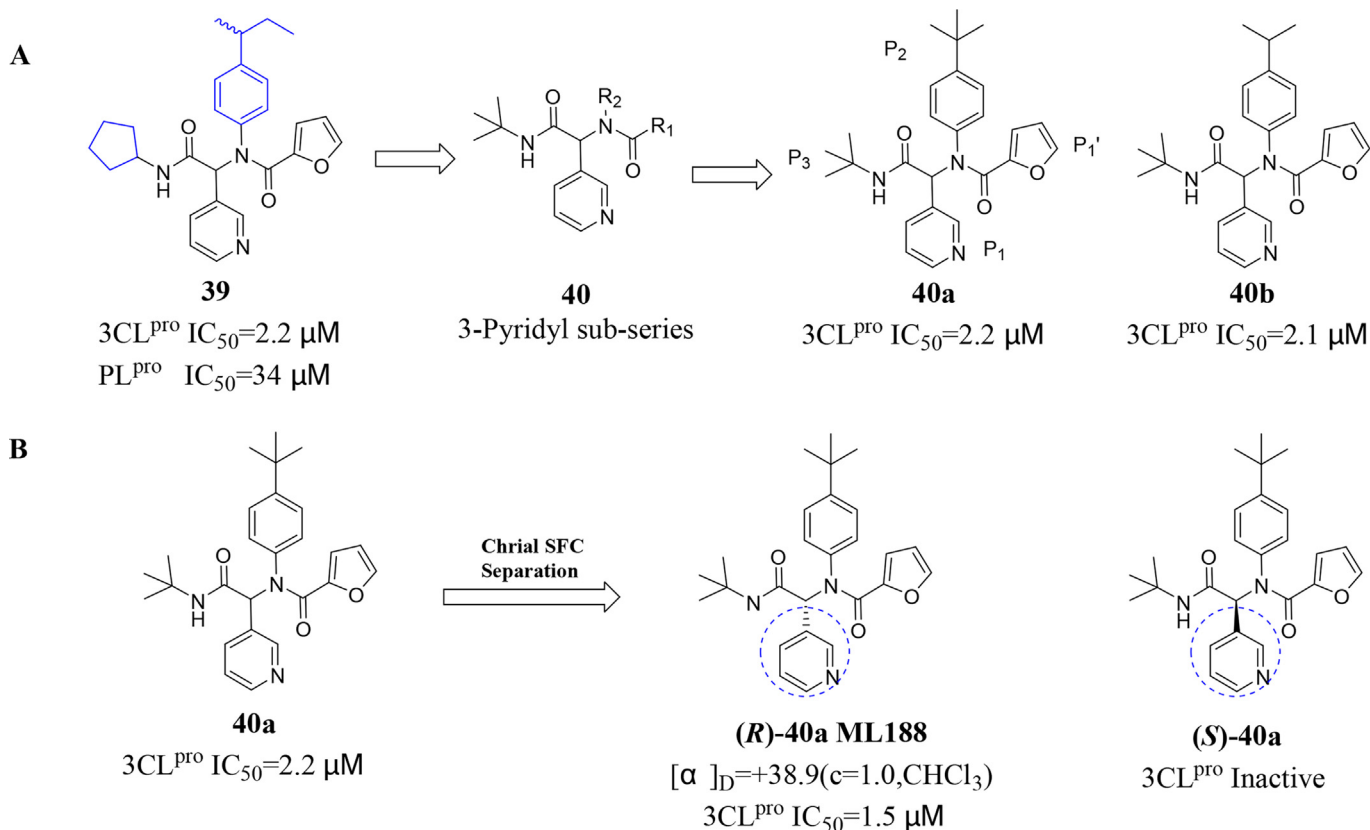


Fig. 8. Octahydro-isochromene scaffold of SARS 3CL^{pro} inhibitors.

Fig. 9. 38 and its binding pocket with SARS 3CL^{pro}.

(approximately 293,000 compounds) to find hits of 3CL^{pro} inhibitors. The analysis of a dipeptide compound library identified **39** (Fig. 10-A), which had an IC_{50} less than 10 μM and was thus considered an exceptionally good candidate. Thus, a series of 3-pyridyl derivatives were subsequently optimized based on hit **39**, and the resulting compounds **40a** ($IC_{50} = 2.2 \mu M$) and **40b** ($IC_{50} = 2.1 \mu M$) exhibited compelling inhibitory activity against SARS-CoV 3CL^{pro}. The X-ray crystal structure of (*R*)-**40a** combined with SARS-CoV 3CL^{pro} (Fig. 11) demonstrated that (*R*)-**40a** preferentially occupied the S1'-S3 3CL^{pro} subpockets. According to the identified binding mode, tert-butyl amide occupies the S3 pocket, the tert-butyl anilido group occupies a deep S2 pocket, and the 3-pyridyl group occupies the S1 pocket.

To further clarify the SAR of the lead compound **40a**, the P1–P3 framework was maintained consistent, whereas a library of five-membered aromatic heterocycles was synthesized through alterations in the P1' position (Table 2, 41a–41f). Among the resulting compounds, imidazole (**41c**, $IC_{50} = 6 \mu M$) and 5-chlorofuran (**41e**, $IC_{50} = 5.2 \mu M$) substituted analogues were found to be the most potent. A subsequent study of P1 replacements was performed to identify alternative hydrogen bond-acceptor groups that might engage His163 while retaining the 2-furyl amide P1' group. Among the six-membered π -excessive heterocycles examined (**42a**–**42c**), pyridazine (**42a**) and pyrazine (**42b**) were well tolerated. Furthermore, chiral stationary-phase supercritical fluid chromatography (SFC) was applied to separate **40a** enantiomers (Fig. 10-B), and

Fig. 10. (A) Primary SAR study of the furyl amide hit compound 39. (B) (*R*)-40a and (*S*)-40a.

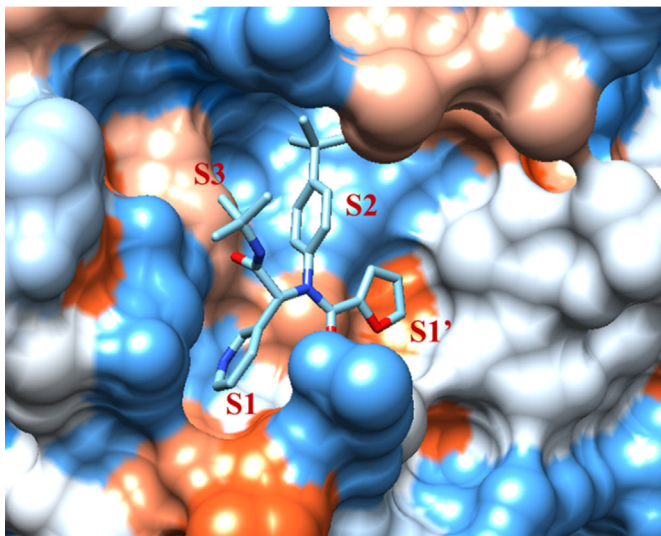


Fig. 11. X-ray crystal structure of (R)-40a bound to SARS-CoV 3CL^{pro} (PDB code: 3V3M).

highly specific inhibition was obtained with a single stereoisomer (**R**-40a (**ML188**)), which exhibited an IC₅₀ of 1.5 ± 0.3 μM.

Further screening revealed that a class of noncovalent benzotriazole inhibitors from the NIH Molecular Libraries Probe Production Centers Network (MLPCN) exhibited improved biological activity [68]. Among these compounds, compound **43** substantially inhibited SARS-CoV 3CL^{pro} (IC₅₀ = 6.2 μM).

According to X-ray crystallography (PDB code: 4MDS, Fig. 12), rearrangement of the Gln189 and Met49 residue side chains forms the diamide **43**, which exhibits an induced-fit binding site. This induced-fit binding site accommodates the *syn* N-methyl pyrrole and anilido acetamide moieties of the inhibitors within the S2–S4 and S2–S1' subpockets, respectively. In addition to the P2–P4 and P2–P1' groups, **43** partially occupies the S3 subpocket with a terminating 2-methylbutylamide. Moreover, Cys145 and benzotriazole N-(2) form a key hydrogen bond near the catalytic centre. Other hydrogen bond interactions are found near the catalytic site of His163 and benzotriazole N-(3), and the main chain Glu-166 NH shows an obvious interaction with the central acetamide oxide.

As a promising hit, the template compound **43** has been subjected to intense derivatization, including P1 modifications, P2–P1' exploration and P3 truncation (Fig. 13). First, the failure of the alteration of P1 to benzimidazole (**44a**–**44c**) indicated a strict substituent requirement for the 1,2,3-triazole unit. Comparatively, 4-phenyl-1,2,3-triazolium **44f** exhibited effective inhibition (IC₅₀ = 11 μM), and unsubstituted triazole **44d** and trimethyl silyl triazole **44e** were ineffective, which demonstrated the importance of maintaining a proper aromatic ring in the P1 subpocket during the optimization. Second, acetamide at the P2–P1' region was exchanged with cyclic and acyclic amide congeners to render a series of analogues with IC₅₀ values below 10 μM, and the *i*-propyl **45b** and cyclobutyl **45d** amide derivatives exhibited compelling activity with IC₅₀ values less than 5 μM. Furthermore, researchers performed fragment truncation at the P3 position to minimize pharmacophores and thereby reduce the overall redundant group and molecular weight, which could improve the physical and chemical properties as well as the ligand binding efficiency. Satisfactorily, the truncated amides **46** exhibit comparable activity to the well-designed diamide counterparts **45** (see Fig. 12 for **45a**–**45d** vs **46a**–**46d**). Karypidou et al. [69] prepared a novel library of fused 1,2,3-triazole [4,5-*c*] pyridine derivatives, and among these, **47**–**51** exhibited good antiviral properties against human coronavirus 229E (Table 3).

4.3. 3CL^{pro} inhibitor with a piperidine moiety

Based on an analysis of the optimization of the lead GC376 (**52**), adduction of an aldehyde bisulphite at the P1' position is necessary for the reaction with the active site Cys148 to generate tetrahedral hemithioacetal. Moreover, the γ-lactam ring at the P1 position and the Leu side chain at the P2 position should be retained and might occupy the S1 and S2 hydrophobic pockets, respectively. Additionally, extending the benzyloxy “cap” to the chlorine-substituted phenylethanol fragment yields GC813 (**53**), and its lower IC₅₀ value can be attributed to an extended conformation and might orient the phenyl ring towards the hydrophobic S4 pocket. As a common privileged scaffold in drug design and discovery, the piperidine moiety is a good design element that can exhibit good interactions with numerous classes of proteins, which would result in optimal pharmacological activity and PK properties [70]. Thus, introducing the high-affinity

Table 2
Variation at the P1' (**41a**–**41f**) and P1 (**42a**–**42c**) sites of **40a** (R&S).

Compound	P1'	3CL ^{pro} IC ₅₀ (μM)	Compound	P1	3CL ^{pro} IC ₅₀ (μM)
41a		39	42a		10
41b		50	42b		5.5
41c		6	42c		45
41d		47			
41e		5.2			
41f		75			

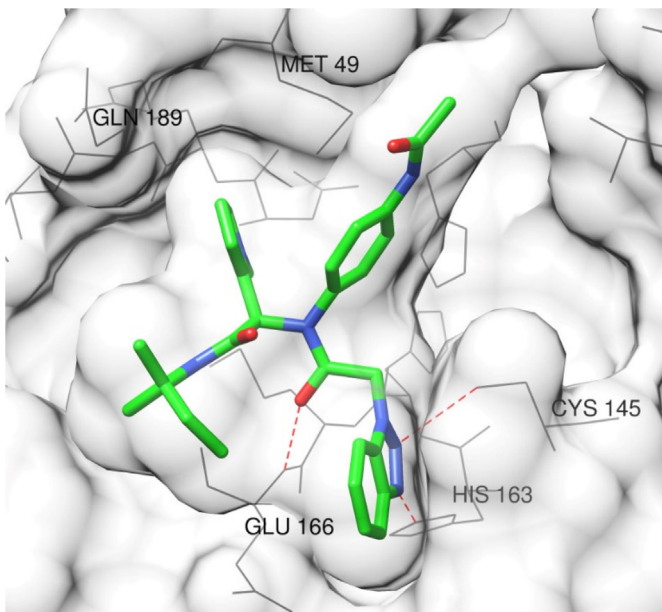


Fig. 12. 43 bound to the binding pocket of SARS-CoV 3CL^{pro} (PDB code: 4MDS).

piperidine moiety into the peptoid scaffold yields a series of structurally novel inhibitors (Table 4, 54a–54f). The piperidine-based design strategy is an effective tactic for rendering a dipeptidyl inhibitor capable of engaging in optimal binding interactions with all four S1–S4 subsites, and the resulting inhibitors have a lower molecular weight and a reduced peptidyl character compared with the tetrapeptidyl inhibitor, which is expected to display enhanced solubility and PK liabilities. Gratifyingly, 54b and 54d, which are representative aldehyde bisulphite compounds, display potent MERS-CoV inhibitory activities with low cytotoxicity ($CC_{50} > 100 \mu\text{M}$).

4.4. Unsymmetrical aromatic disulphides

Unsymmetrical aromatic disulphide compounds are a class of inhibitors that exert significant inhibitory effects on SARS 3CL^{pro} [71]. These new chemical entities display excellent IC₅₀ values in the range of 0.516–5.954 μM (Fig. 14, compounds 55–59). Preliminary studies have indicated that these disulphides are reversible and competitive inhibitors. Among these disulphides, the representative compound 55 binds to SARS-CoV 3CL^{pro} via multiple hydrogen-bonding and hydrophobic contacts. Phe140, Leu141, His163, Met165, Glu166 and His172 form hydrophobic interactions with 55, whereas Asn142, Gly143 and Cys145 form intermolecular hydrogen bonds with 55 (Fig. 15).

4.5. Serine derivatives

To develop nonpeptidic inhibitors that interact with the P1, P2 and P4 sites of 3CL^{pro}, a new series of serine derivatives were designed by Kenichi Akaji et al. based on the tetrapeptide aldehyde Ac-Thr-Val-Cha-His-H (60, IC₅₀ = 98 nM) and Bai's bis-cinnamoyl inhibitor (IC₅₀ = 10.6 μM) [72,73]. First, imidazole, cyclohexyl, and hydroxyl groups, which were previously reported in the literature and exhibit potent biological activity, were linked to L-serine for the design of serine derivatives (61,62), as shown in Fig. 16. However, compared with peptide inhibitor 83, these optimized groups did not provide good coverage of the substrate-recognition pocket of 3CL^{pro} (PDB code: 3AW1), and the different binding modes of peptide inhibitors and non-peptide inhibitors with

3CL^{pro}s lead to changes in the interactions between these groups and the corresponding pocket [74]. It was hypothesised that the cyclohexyl group would occupy the S2 pocket of 3CL^{pro}, but contrary to the expectations, molecular mechanics calculations and docking simulations indicated that the cyclohexyl group of serine derivatives (61, 62) must occupy the S1 pocket of 3CL^{pro}. Thus, the imidazole and hydroxyl groups of 61 and 62, which are expected to interact with the S1 and S4 pockets, were not effective and thereby reduced the interaction between the inhibitor and 3CL^{pro}. In addition, Bai's inhibitor 63 is located deep insides the S'1, S1 and S2 pockets and exhibits appropriate cinnamoyl functionalities [75]. Therefore, benzoyl and aniline groups were used to molecularly dock with serine derivatives to obtain 64. In addition, reasonable structural transformations of the serine derivative and hybrids constructed with other functionalities were investigated. Virtual screening using GOLD software indicated that N-cinnamoyl derivatives with benzoate, such as 64 and 65, are suitable substructures.

Based on the embedding of the substrate recognition pocket of the SARS 3CL^{pro} R188I mutant (PDB code: 3AW1), the isoserine skeleton was found to exhibit a more reasonable interaction with the mutant 3CL^{pro}, resulting in the isoserine derivative (*R*)-66, which might be obtained by replacing the amine group at the α -position and adding a hydroxy group at the β -position of 65. The docking simulation of (*R*)-66 with SARS 3CL^{pro} revealed a hydrophobic space on the S2 pocket of the R188I mutant protease. Compared with hydrophobic functional groups (such as alkane, cycloalkane and aromatic rings), the phenyl group was more suitable for insertion into the S2 pocket of the R188I mutant protease; therefore, (2*R*,3*S*)-phenylisoserine (PIS) derivative 67 was obtained and selected as a candidate compound. A SAR study of the PIS derivative and the corresponding S1' pocket revealed that the inclusion of a cinnamic derivative (68a, 68b) or a phenyl propionate derivative (68c) at the P1' position elevated the inhibitory activity, with IC₅₀ values ranging from 65 to 75 μM (Fig. 17). In addition, cyclohexyl rings are essential to the P1 function of PIS scaffolds, whereas the cinnamyl functional group at P4 can effectively maintain the inhibitory strength.

4.6. Pyrazolone and pyrimidines

Based on the 1,3,4,5-tetraaryl-substituted pyrazole 69 identified through high-throughput screening, a series of 1,3,4-triple substituted pyrazolinone compounds were designed and synthesized as SARS-CoV 3CL^{pro} inhibitors. Among the resulting compounds (Fig. 18), 70–73 exerted strong inhibitory effects on SARS-CoV 3CL^{pro}, with IC₅₀ values of 5.5, 10.8, 6.8 and 8.4 μM , respectively, and favourably, 73 could also effectively inhibit coxsackievirus B3 3CL^{pro} [76]. Po-Huang Liang et al. further synthesized a series of analogues by grafting the neuraminidase (NA) inhibitor phenyl furan moiety into a 1,3,4-triple substituted pyrazolinone nucleus [77]. Among the resulting series, compounds 74d–74f showed comparable inhibitory activity against SASR and MERS 3CL^{pro}s. In addition to the catalytic residue Cys145, the S1 subsite of 3CL^{pro} also included another important component, the oxyanion hole. This component is formed by the interaction of the C-terminal carboxylate anion of the conserved Gln with Gly143, Ser144 and Cys145, which stabilizes the transition state during proteolysis. Docking studies have indicated that the carboxylates present at the A or D ring are critical for disrupting the stability of the oxyanion hole in 3CL^{pro}. Further SAR studies have shown that the pharmacophores phenyl at R₃ (74a vs 74b) and a carboxylate at either R₁ or R₄ (74c vs 74d) are essential for the activity (Fig. 18). Because the modification of rings A and B is tolerated well, the D ring can be further altered to enhance the activity of the compounds.

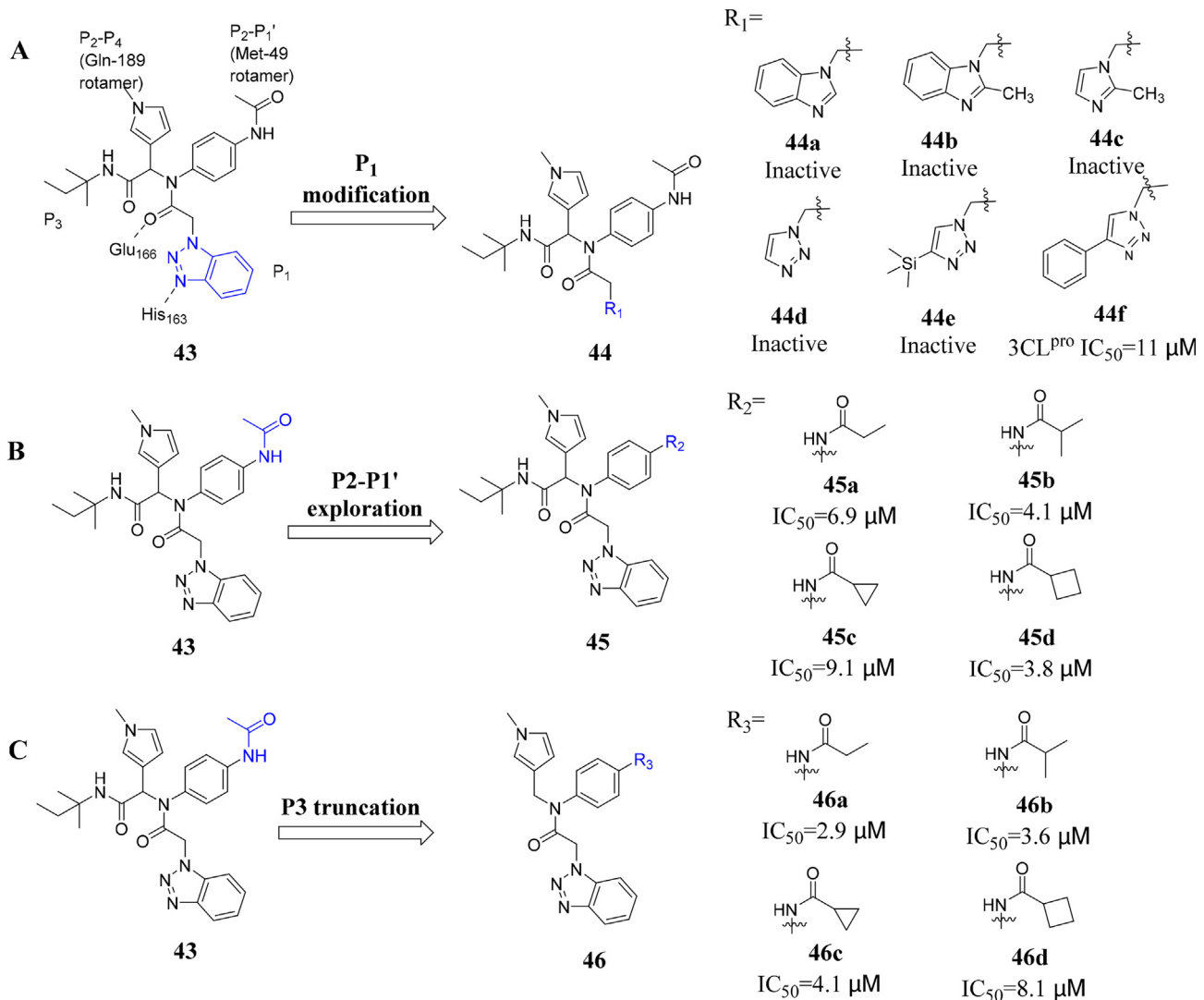


Fig. 13. (A) P1 modifications, (B) P2–P1' exploration and (C) P3 truncation of the hit compound 43.

Table 3

Anti-coronavirus (229E) activities of 1,2,3-triazole [4,5-c] pyridine derivatives.

Compound	R ₁	R ₂	EC ₅₀ (μM)	Compound	R	R'	EC ₅₀ (μM)
47		H	8.95	50		H	8.9
48		H	9.45	51		H	11.95
49			9.45				

Another series of 2-(benzylthio)-6-oxo-4-phenyl-1,6-dihydropyrimidines (**75a**–**75f**) also showed encouraging results as new anti-SARS hits [78]. The cytotoxicity of the test compounds

was assessed using the MTT assay, and all the compounds were devoid of cytotoxicity. Further SAR studies revealed that compound **75c**, which has a nitro at the C-4 position, is the most potent

Table 4
Evolution of the inhibitors **54a–54f**.

Compound	R ₃	R ₄	X	IC ₅₀ (μM)	
				MERS-CoV	SARS-CoV
52 GC376 EC ₅₀ =0.9 μM					
53 GC813 EC ₅₀ =0.5 μM					
54a	H	Boc	CHO	0.6	2.1
54b			CH(OH)SO ₃ Na	0.4	5.1
54c	(C ₆ H ₅)CH ₂	Boc	CHO	0.8	5.2
54d			CH(OH)SO ₃ Na	0.7	6.3
54e	H	CH ₃ CH ₂ O(CO)	CHO	0.6	3.2
54f			CH(OH)SO ₃ Na	0.5	8.8

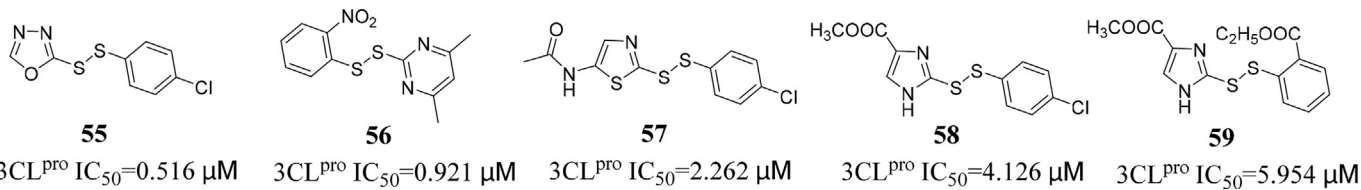


Fig. 14. Unsymmetrical aromatic disulphides.

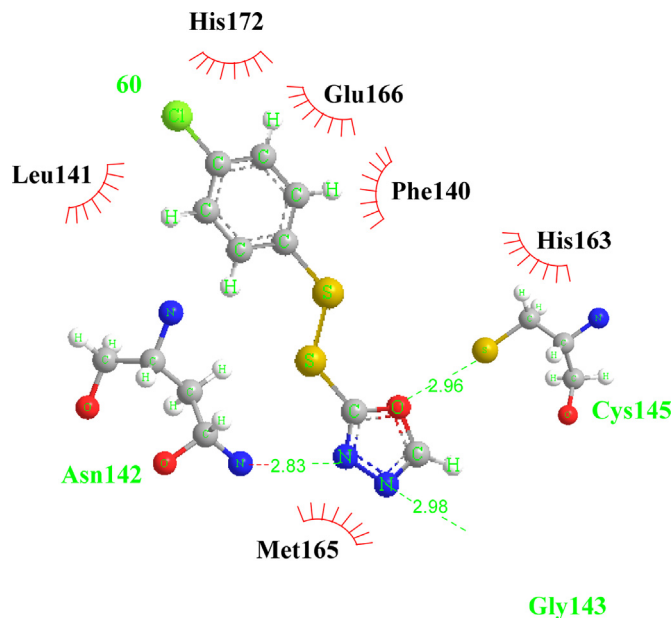


Fig. 15. Modelling of **55** with SARS CoV 3CL^{pro}. The hydrogen bonds between the enzyme and the inhibitor are shown as green dashed lines, and the distances are shown in units of Å. The amino acid residues that contribute to van der Waals contacts with the inhibitor are shown as red arcs. (For interpretation of the references to colour in this figure legend, the reader is referred to the Web version of this article.)

inhibitor of SARS-CoV 3CL^{pro} ($IC_{50} = 6.1 \mu M$). The moderate electron-withdrawing substituent at R₁, such as chloro, in compounds **75c** and **75d** improved the inhibitory activity compared with the presence of electron-donating groups, such as methyl and methoxy groups (as shown in Table 5). Molecular docking results have illustrated (docking study of **75c** with PDB code: 1UK4) that

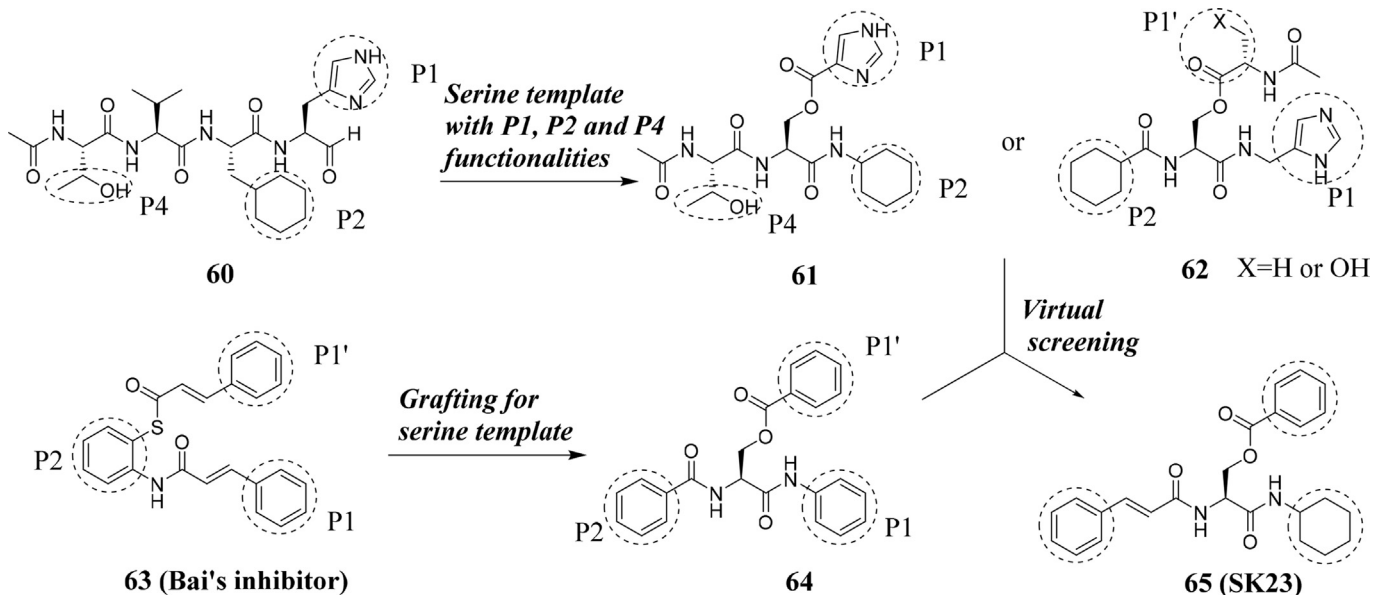
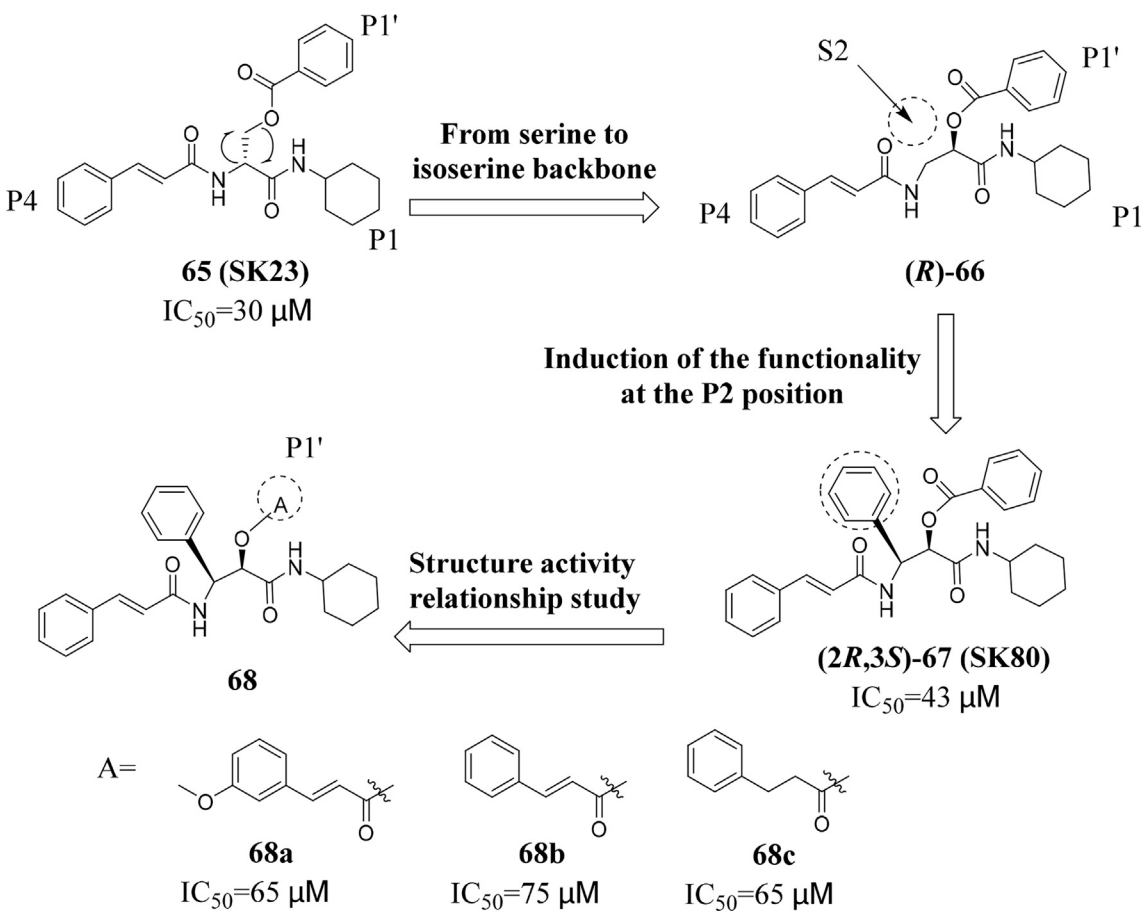
the distance between the NH of the pyrimidine ring and the oxygen atom of Glu-166 was constrained by 2.0 Å. The orientation of the ligand has a nitro phenyl group situated in the S1 pocket, and the nitro group points towards the surface of the protein. The oxygen of the nitro group forms a hydrogen bond with Gly143 and Cys145, and the chlorophenyl ring fits into the S2 pocket and forms hydrophobic interactions with Met49 and Gln189.

4.7. Natural product derivatives

4.7.1. Flavonoids, biflavonoids and chalcones

Quercetin (**76**), epigallocatechin gallate (**77**) and gallicatechin gallate (**78**, GCG) also show mild inhibitory effects against SARS-CoV 3CL^{pro}, with IC₅₀ values of 73 μM, 73 μM and 47 μM, respectively (Fig. 19). In addition, **78** exhibits competitive inhibition towards 3CL^{pro}, with a Ki value of 25 μM. According to the results from a docking analysis, the galloyl acyl moiety at the 3-OH position of compound **78**, which occupies the S1 pocket, is essential for inhibitory activity against 3CL^{pro} [79]. A series of inhibitors were isolated and purified from the leaves of *Torreya nucifera* (Fig. 19). According to a preliminary screen, the biflavone amentoflavone (**79**) ($IC_{50} = 8.3 \mu M$) exerted the most potent inhibitory effect against 3CL^{pro}. A SAR study based on these flavonoids found that a methoxy substitution at the C-7 position could enhance the inhibitory effect. Specifically, the C-7 methoxy-substituted compounds **80** ($IC_{50} = 32.0 \mu M$) and **81** ($IC_{50} = 38.4 \mu M$) exhibited two-fold higher inhibitory activity against SARS-CoV 3CL^{pro} compared with that of **82** ($IC_{50} = 72.3 \mu M$) [80].

Another series of chalcones (Figs. 19, 83–85) isolated from *Angelica keiskei* were evaluated in terms of their anti-SARS 3CL^{pro} activity. Chalcone **84**, which contains perhydroxyl groups, exhibited the most potent inhibitory activity against 3CL^{pro}, with an IC₅₀ value of 11.4 μM. A detailed ligand-protein mechanistic analysis indicated that the chalcones exhibited competitive inhibition with SARS-CoV 3CL^{pro} [81].

Fig. 16. Design scheme of serine derivatives **64** and **65**.Fig. 17. Evolution of phenyl isoserine derivatives **68a**, **68b**, and **68c** from serine derivatives.

4.7.2. Isatin derivatives

Previous studies have shown that isatin and its derivatives have a wide range of antiviral and antibacterial activities [82–84], including anti-HIV virus [85,86], anti-hepatitis C virus (HCV) [87],

anti-mycobacterium tuberculosis and anti-pathogenic activities [88,89]. In addition, isatin derivatives are good candidates for the development of anti-coronavirus drugs [90]. For anti-coronavirus drug discovery, a series of synthetic 5-sulfonyl isatin derivatives

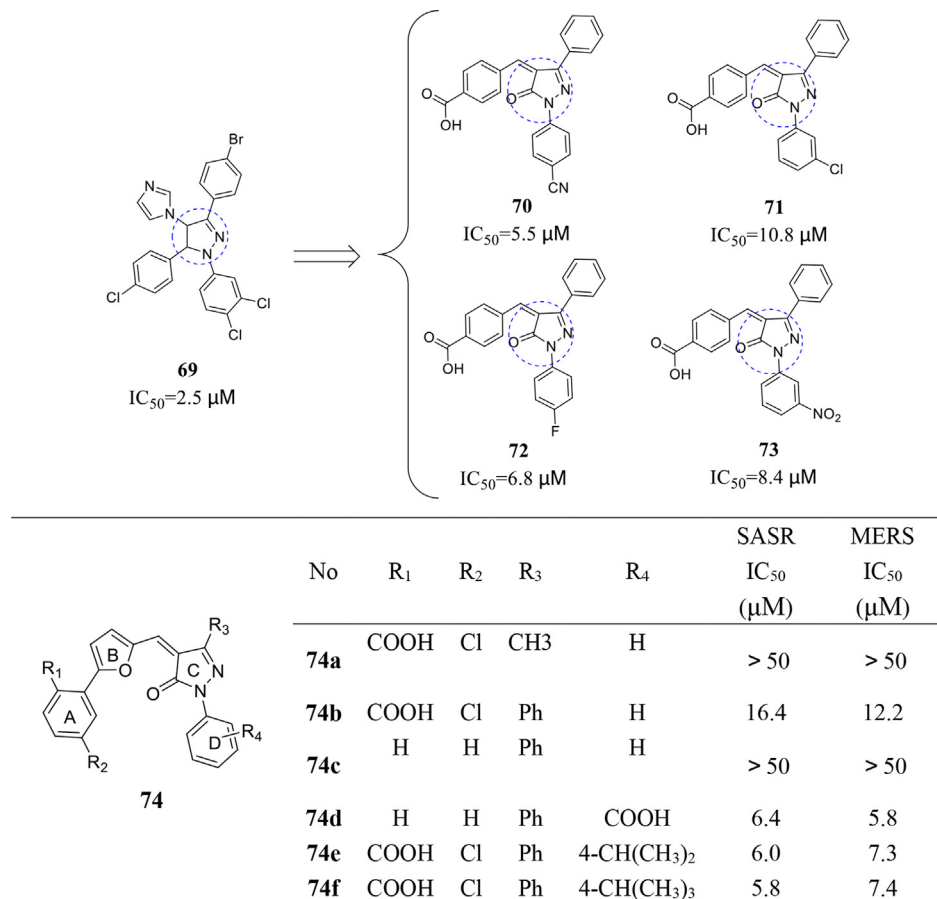
Fig. 18. Structure of pyrazolones and their inhibition of SARS and MERS 3CL^{pro}.

Table 5
Structure and activity of compounds 75a-75f.

No	R ₁	R ₂	n	SASR IC ₅₀ (μM)
75a	4-OCH ₃	4-NO ₂	1	26.3
75b	4-CH ₃	4-NO ₂	1	>50
75c	4-Cl	4-NO ₂	1	6.1
75d	4-Cl	H	2	16.9
75e	3-NO ₂	4-NO ₂	1	10.6
75f	3-NO ₃	H	2	>50

(86–92) were reported as noncovalent SARS M^{pro} inhibitors [91]. These isatin derivatives inhibited SARS-CoV 3CL^{pro} at the low micromolar range, and **86** (IC₅₀ = 1.04 μM) was found to be the most potent. SAR studies revealed that the piperidin sulfonyl-substituted compounds **86–89** exerted a more significant inhibitory effect against 3CL^{pro} (IC₅₀ < 5 μM) than the piperazine sulfonyl-substituted isatins **90–92**. Among the former, the 4-methyl piperidin sulfonyl (**87**, IC₅₀ = 1.18 μM) and 2-methyl piperidin sulfonyl (**88**, IC₅₀ = 2.25 μM) isatin derivatives were identified as the optimal candidates.

4.7.3. Terpenoid derivatives

A screening of natural products for the identification of anti-coronavirus 3CL^{pro} inhibitors revealed that tanshinone-type diterpenes (compounds **93–99**) derived from *Salvia miltiorrhiza* are selective inhibitors of SARS-CoV 3CL^{pro} and PL^{pro} [92]. With the exception of cryptotanshinone (**96**), the other isolated tanshinones

exerted a dose-dependent inhibitory effect but no time-dependent effect against 3CL^{pro}. The activity of **93–99** against 3CL^{pro} ranged from 14.4 to 89.1 μM. Further SAR study revealed that subtle differences in the substituents and stereo configuration can substantially affect the inhibitory activity. Specifically, the presence of a naphthalene moiety in the diterpene quinolone backbone appeared to improve the inhibition of 3CL^{pro} in compared with that obtained with dimethyl-substituted tetralin (**97** and **98** vs **93** and **96**). In addition, the dihydrofuran group (**96**) on ring A of cryptotanshinone reduced the inhibitory activity by two-fold compared with that of tanshinones (**93–95**) containing a furan group.

Additionally, celastrol (**100**), pristimerin (**101**), tingenone (**102**), and iguesterin (**103**) were isolated from *Tripterygium regelii* and showed favourable competitive inhibitory activities against SARS-CoV 3CL^{pro} with IC₅₀ values of 2.6, 9.9, 5.5 and 10.3 μM, respectively [93]. Dihydrocelastrol (**104**) was synthesized by hydrogenation under a palladium catalyst, but its 3CL^{pro} inhibitory activity on SARS 3CL^{pro} was relatively weak. Further SAR research indicated that a quinone-methide moiety in the A ring and a more hydrophobic E ring could promote inhibitory activity against 3CL^{pro}.

5. Discussion and perspectives

As the cases of SARS-CoV-2 infections continue to rise, the development of effective drugs and vaccines for the targeted treatment of COVID-19 is becoming increasingly urgent. Among the few available targets for anti-coronavirus drug development, 3CL^{pro}, which is a key protein involved in the replication and transcription of coronaviruses, has become an important and

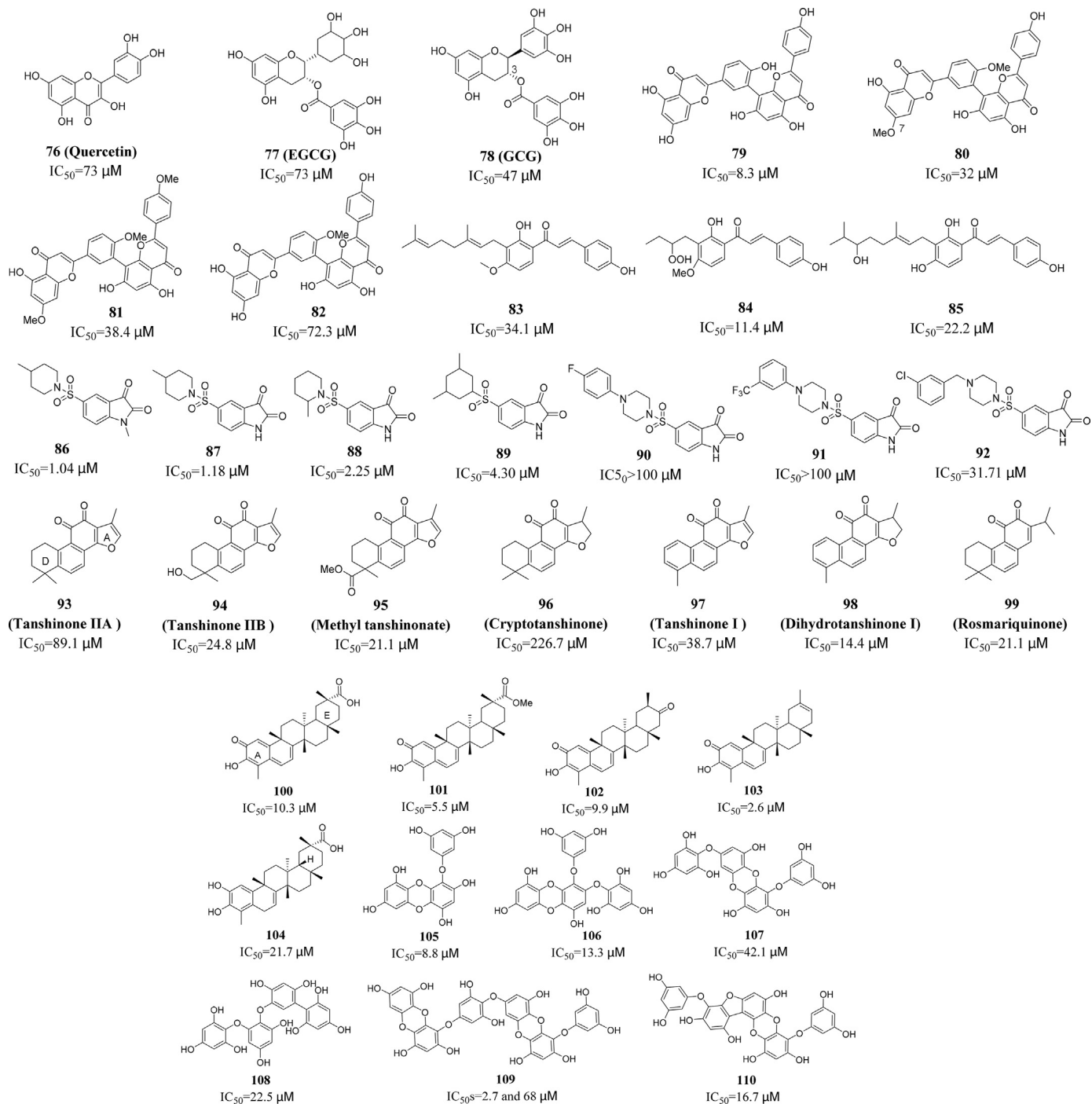


Fig. 19. Chemical structures of natural product derivatives **76–110**.

relatively mature drug target in anti-coronavirus drug research. In addition, the SARS-CoV-2 3CL^{Pro} crystal structure (PDB code: 6LU7) is the first non-structural functional protein of SARS-CoV-2 that has a confirmed conserved structure compared with those of SARS and MERS 3CL^{Pro}s. Thus, broad-spectrum coronavirus 3CL^{Pro} inhibitors are particularly suitable for the treatment of current and future coronavirus epidemics. The present article reviews the research progress on coronavirus 3CL^{Pro} inhibitors discovered from various sources over the past 10 years (2010–2020), including synthetic peptidomimetic and nonpeptidic inhibitors and natural product derivatives, and attempts to provide a complete description of the

structural characteristics of 3CL^{Pro} inhibitors, including details on their binding modes and other related information.

Herein, the structural characteristics, binding modes and SARs of recent coronavirus 3CL^{Pro} inhibitors are fully described. The warhead groups of peptidomimetic inhibitors mainly include aldehydes, ketones and different types of Michael receptors. These covalent irreversible inhibitors mainly utilize warhead functional groups to covalently bond with Cys145 residues in the 3CL^{Pro} S1' pocket and thereby exert relatively durable inhibitory effects. The published studies have shown that covalent irreversible 3CL^{Pro} inhibitors exhibit significantly improved antivirus activity, and some

inhibitors can even achieve effects at nanomolar levels. However, covalent inhibitors exhibit potential off-target problems and toxic side effects. Although the recent studies on peptidomimetic inhibitors are fewer than those that investigated nonpeptidic inhibitors, the aldehyde compounds **11** and **12** and α -ketoamide compounds (**25–27**), which are among the recently reported peptidomimetic 3CL^{pro} inhibitors, exhibit excellent inhibitory activity against SARS-CoV-2. Inhibitor **11** is one of the most effective inhibitors among the aldehyde peptide series. Thus, the toxicity of inhibitor **11** over a 7-day period has been studied at different doses, specifically at dosing levels of 2, 6, and 18 mg/kg on SD rats and at a dose range of 10–40 mg/kg on beagle dogs, and all the tested animals showed significant toxicity after the inhibitor was administered once a day (QD) via intravenous drip. Therefore, **11** might be a good candidate for further COVID-19 clinical research. Coincidentally, the pharmacokinetic characteristics of compound **26** indicated obvious lung affinity, and this compound is suitable for administration via inhalation. Therefore, the pyridone-containing compound **26** might become another lead for further COVID-19 pandemic research.

Correspondingly, noncovalent reversible 3CL^{pro} inhibitors mainly exhibit weak reversible binding (such as hydrogen bonds, van der Waals forces, and hydrophobic forces) with the amino acid residues in the S1, S2, and S4 pockets, which sometimes includes the catalytically active Cys145 in the S1' pocket. This weak reversible binding could result in avoidance of the off-target risk and

toxicity of irreversible inhibitors, and thus, these inhibitors might be suitable for long-term administration. Among the nonpeptidic reversible inhibitors, **55–59**, which contain a piperidine moiety, and **54a–54f**, which contain unsymmetrical aromatic disulphides, demonstrate excellent inhibitory activity. Some natural products and derivatives, such as isatin [94], flavonoids, and tanshinone, might also be good candidates for the development of anti-coronavirus drugs. Specifically, **46a**, **54a**, **74d** and **75c** are non-covalent SARS-CoV 3CL^{pro} inhibitors with a medium molecular weight and good antiviral activity and can potentially be utilized as lead templates for further drug design and screening.

However, 3CL^{pro} noncovalent inhibitors also have some shortcomings, such as drug effects that are not strong and/or durable, which means that these noncovalent inhibitors would need to be administered at high dosages or multiple times. Non-covalent inhibitors can also result in the emergence of resistance after their long-term administration. Based on a review of the advantages and disadvantages of both covalent and noncovalent inhibitors of 3CL^{pro}, we recommend that reversible covalent inhibitors of 3CL^{pro} constitute a new research direction. Specifically, the Michael warhead can be replaced by cyano (or trifluoromethyl), which might result in the formation of a reversible covalent bond with the Cys145 residue, which is unique to the coronavirus 3CL^{pro} S1' pocket, and this binding can potentially reduce the “off-target” risk and toxic side effects while enhancing the efficacy [95–98].

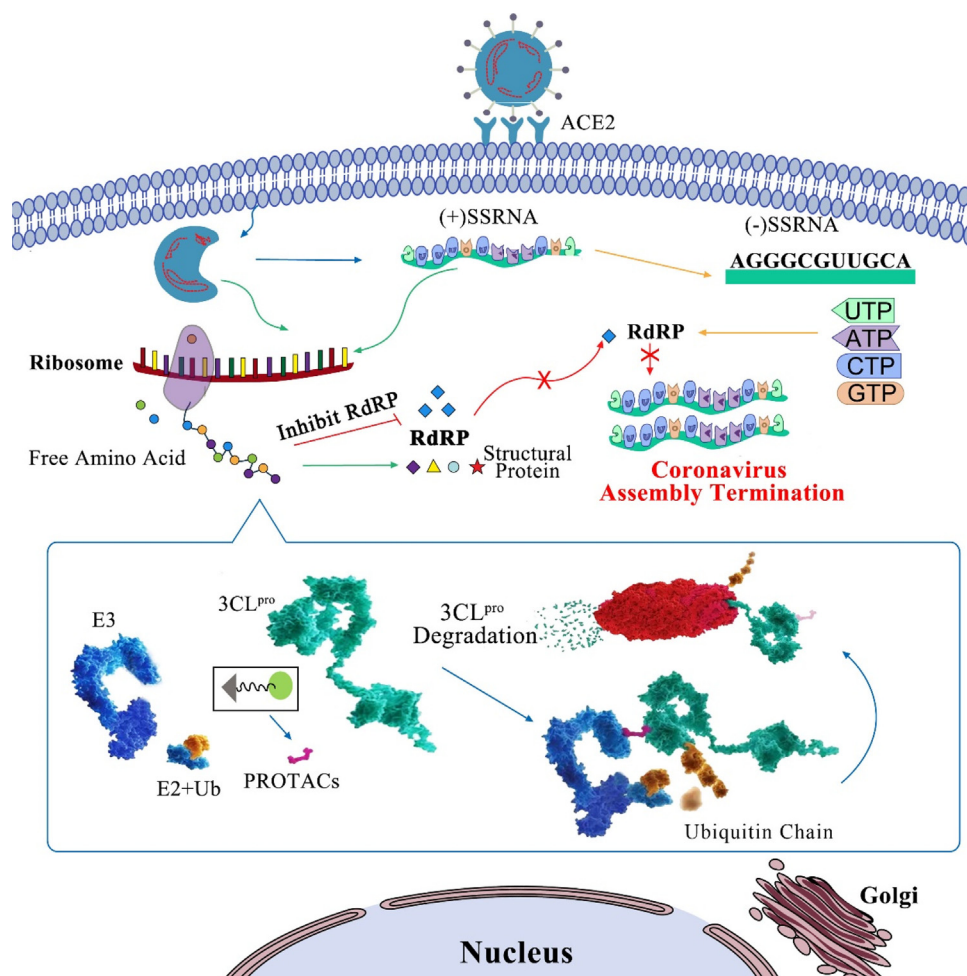


Fig. 20. Illustration of PROTACs targeting the degradation of 3CL^{pro} and thereby inhibiting coronavirus assembly and replication.

Further analyses of the previous studies on 3CL^{PRO} inhibitors in association with the booming research on PROTACs [99,100] have led to the emergence of the following drug development ideologies. PROTAC technology can be used in the design of anti-coronavirus drugs that induce the intracellular degradation of functional nsps of exogenous viruses. The principle of PROTAC technology involves the use of a bifunctional small molecule to links the target protein and the E3 ligase in the cell such that the target protein is ubiquitinated, and the ubiquitinated protein is then recognized by the proteasome, which leads to degradation of the target protein [101]. To date, various endogenous proteins, such as BTK, PARP1, HDAC6, AR, ER, BET, BRD4, BRD9, RIPK2, TBK1, Sirt2, CDK9, p38 α , pirin, c-Met, EGFR, FAK, and FLT3, have been reportedly degraded using PROTAC technology [102–106]. However, the application of PROTAC technology for the degradation of foreign proteins (such as viral proteins) remains in its infancy. To date, only the NS3/4A protease degrader DGY-08-097 of HCV has been reported, and its antiviral activity and resistance characteristics are significantly superior to those of the traditional drug telaprevir [107]. Thus, we propose that the existing 3CL^{PRO} inhibitors can be combined with PROTAC technology to develop coronavirus 3CL^{PRO} PROTACs. These PROTAC degraders could exhibit the advantages of both occupancy-driven 3CL^{PRO} inhibitors and those of event-driven PROTACs: low-dose exposure would result in multiple rounds of 3CL^{PRO} degradation and would avoid the intracellular accumulation of 3CL^{PRO} in infected cells. These procedures would completely block the biological function of coronavirus 3CL^{PRO} and its downstream viral proteins and would therefore inhibit the assembly and replication of the coronavirus in infected cells (shown in Fig. 20). Reversible covalent PROTACs for 3CL^{PRO} have been designed and synthesized in our laboratory for further screening, and we expect that these inhibitors will overcome the shortcomings of traditional 3CL^{PRO} inhibitors and take advantage of the degradation effects of PROTACs.

Declaration of competing interest

The authors declare that they have no known competing financial interests or personal relationships that could have appeared to influence the work reported in this paper.

Acknowledgements

This work was supported by the National Natural Science Foundation of China (grant nos. 81602967 and 81803784), the China Postdoctoral Science Foundation (grant nos. 2016M592898XB and 2019M663921XB), the Basic Research Program of Natural Science of Shaanxi Province (grant nos. 2019JQ-779, 2020CGXNG-044, 19JC006, 2019JQ-484 and 2019JQ-252), the Basic Research Plan of the Education Department of Shaanxi Province (grant no. 19JC006), and the College Students' Innovative Entrepreneurial Training Program (grant nos. 201510708172, 201610708019, and 2019107080827).

References

- [1] F. Wu, S. Zhao, B. Yu, Y. Chen, W. Wang, Z. Song, Y. Hu, Z. Tao, J. Tian, Y. Pei, A new coronavirus associated with human respiratory disease in China, *Nature* 579 (2020) 265–269.
- [2] J.T. Wu, K. Leung, G.M. Leung, Nowcasting and forecasting the potential domestic and international spread of the 2019-nCoV outbreak originating in Wuhan, China: a modelling study, *Lancet (London, England)* 395 (2020) 689–697.
- [3] D.S. Hui, I.A. E., T.A. Madani, F. Ntoumi, R. Kock, O. Dar, G. Ippolito, T.D. McHugh, Z.A. Memish, C. Drosten, A. Zumla, E. Petersen, The continuing 2019-nCoV epidemic threat of novel coronaviruses to global health – the latest 2019 novel coronavirus outbreak in Wuhan, China, *Int. J. Infect. Dis. : IJID : Off. Publ. Int. Soc. Infect. Dis.* 91 (2020) 264–266.
- [4] J.T. Wu, K. Leung, G.M. Leung, Nowcasting and forecasting the potential domestic and international spread of the 2019-nCoV outbreak originating in Wuhan, China: a modelling study, *Lancet* 395 (2020) 689–697.
- [5] J.F. Chan, S. Yuan, K.H. Kok, K.K. To, H. Chu, J. Yang, F. Xing, J. Liu, C.C. Yip, R.W. Poon, H.W. Tsui, S.K. Lo, K.H. Chan, V.K. Poon, W.M. Chan, J.D. Ip, J.P. Cai, V.C. Cheng, H. Chen, C.K. Hui, K.Y. Yuen, A familial cluster of pneumonia associated with the 2019 novel coronavirus indicating person-to-person transmission: a study of a family cluster, *Lancet (London, England)* 395 (2020) 514–523.
- [6] P. Zhou, X.L. Yang, X.G. Wang, B. Hu, L. Zhang, W. Zhang, H.R. Si, Y. Zhu, B. Li, C.L. Huang, H.D. Chen, J. Chen, Y. Luo, H. Guo, R.D. Jiang, M.Q. Liu, Y. Chen, X.R. Shen, X. Wang, X.S. Zheng, K. Zhao, Q.J. Chen, F. Deng, L.L. Liu, B. Yan, F.X. Zhan, Y.Y. Wang, G.F. Xiao, Z.L. Shi, A pneumonia outbreak associated with a new coronavirus of probable bat origin, *Nature* 579 (2020) 270–273.
- [7] C. Huang, Y. Wang, X. Li, L. Ren, J. Zhao, Y. Hu, L. Zhang, G. Fan, J. Xu, X. Gu, Clinical features of patients infected with 2019 novel coronavirus in Wuhan, China, *Lancet* 395 (2020) 497–506.
- [8] J. Cui, F. Li, Z. Shi, Origin and evolution of pathogenic coronaviruses, *Nat. Rev. Microbiol.* 17 (2019) 181–192.
- [9] S. van Boheemen, M. de Graaf, C. Lauber, T.M. Bestebroer, V.S. Raj, A.M. Zaki, A.D.M.E. Osterhaus, B.L. Haagmans, A.E. Gorbalenya, E.J. Snijder, R.A.M. Fouchier, Genomic characterization of a newly discovered coronavirus associated with acute respiratory distress syndrome in humans, *mBio* 3 (2012) e00473-00412.
- [10] V. Nukoolkarn, V.S. Lee, M. Malaisree, O. Aruksakulwong, S. Hannongbua, Molecular dynamic simulations analysis of ritonavir and lopinavir as SARS-CoV 3CL(pro) inhibitors, *J. Theor. Biol.* 254 (2008) 861–867.
- [11] X. Xu, P. Chen, J. Wang, J. Feng, H. Zhou, X. Li, W. Zhong, P. Hao, Evolution of the novel coronavirus from the ongoing Wuhan outbreak and modeling of its spike protein for risk of human transmission, *Science China, Life Sci.* 63 (2020) 457–460.
- [12] R. Ramajayam, K.P. Tan, P.H. Liang, Recent development of 3C and 3CL protease inhibitors for anti-coronavirus and anti-picornavirus drug discovery, *Biochem. Soc. Trans.* 39 (2011) 1371–1375.
- [13] Z. Ren, L. Yan, N. Zhang, Y. Guo, C. Yang, Z. Lou, Z. Rao, The newly emerged SARS-like coronavirus HCoV-EMC also has an "Achilles' heel": current effective inhibitor targeting a 3C-like protease, *Protein Cell* 4 (2013) 248–250.
- [14] X.D. Wu, B. Shang, R.F. Yang, H. Yu, Z.H. Ma, X. Shen, Y.Y. Ji, Y. Lin, Y.D. Wu, G.M. Lin, L. Tian, X.Q. Gan, S. Yang, W.H. Jiang, E.H. Dai, X.Y. Wang, H.L. Jiang, Y.H. Xie, X.L. Zhu, G. Pei, L. Li, J.R. Wu, B. Sun, The spike protein of severe acute respiratory syndrome (SARS) is cleaved in virus infected Vero-E6 cells, *Cell Res.* 14 (2004) 400–406.
- [15] D. Wrapp, N. Wang, K.S. Corbett, J.A. Goldsmith, C.L. Hsieh, O. Abiona, B.S. Graham, J.S. McLellan, Cryo-EM structure of the 2019-nCoV spike in the prefusion conformation, *Science* 367 (2020) 1260–1263.
- [16] S. Skariyachan, S.B. Challapalli, S. Packirisamy, S.T. Kumargowda, V.S. Sridhar, Recent aspects on the pathogenesis mechanism, animal models and novel therapeutic interventions for Middle East respiratory syndrome coronavirus infections, *Front. Microbiol.* 10 (2019) 569.
- [17] S. Mustafa, H. Balkhy, M.N. Gabere, Current treatment options and the role of peptides as potential therapeutic components for Middle East Respiratory Syndrome (MERS): a review, *J. Infect. Public Health* 11 (2017) 9–17.
- [18] D.S. Hui, E.I. Azhar, Y.J. Kim, Z.A. Memish, M.D. Oh, A. Zumla, Middle East respiratory syndrome coronavirus: risk factors and determinants of primary, household, and nosocomial transmission, *Lancet. Infect. Dis.* 18 (2018) e217–e227.
- [19] J. Ziebuhr, Molecular biology of severe acute respiratory syndrome coronavirus, *Curr. Opin. Microbiol.* 7 (2004) 412–419.
- [20] P.A. Rota, M.S. Oberste, S.S. Monroe, W.A. Nix, R. Campagnoli, J.P. Icenogle, S. Peñaranda, B. Bankamp, K. Maher, M.H. Chen, S. Tong, A. Tamin, L. Lowe, M. Frace, J.L. DeRisi, Q. Chen, D. Wang, D.D. Erdman, T.C. Peret, C. Burns, T.G. Skiazeck, P.E. Rollin, A. Sanchez, S. Liffick, B. Holloway, J. Limor, K. McCaustland, M. Olsen-Rasmussen, R. Fouchier, S. Günther, A.D. Osterhaus, C. Drosten, M.A. Pallasch, L.J. Anderson, W.J. Bellini, Characterization of a novel coronavirus associated with severe acute respiratory syndrome, *Science* 300 (2003) 1394–1399.
- [21] C. Drosten, S. Günther, W. Preiser, S. van der Werf, H.R. Brodt, S. Becker, H. Rabenau, M. Panning, L. Kolesnikova, R.A. Fouchier, A. Berger, A.M. Burguière, J. Cinatl, M. Eickmann, N. Escriou, K. Grywna, S. Kramme, J.C. Manuguerra, S. Müller, V. Rickerts, M. Stürmer, S. Vieth, H.D. Klenk, A.D. Osterhaus, H. Schmitz, H.W. Doerr, Identification of a novel coronavirus in patients with severe acute respiratory syndrome, *N. Engl. J. Med.* 348 (2003) 1967–1976.
- [22] J. Cui, F. Li, Z.L. Shi, Origin and evolution of pathogenic coronaviruses, *Nat. Rev. Microbiol.* 17 (2019) 181–192.
- [23] M.A. Marra, S.J. Jones, C.R. Astell, R.A. Holt, A. Brooks-Wilson, Y.S. Butterfield, J. Khattar, J.K. Asano, S.A. Barber, S.Y. Chan, A. Cloutier, S.M. Coughlin, D. Freeman, N. Girn, O.L. Griffith, S.R. Leach, M. Mayo, H. McDonald, S.B. Montgomery, P.K. Pandoh, A.S. Petrescu, A.G. Robertson, J.E. Schein, A. Siddiqui, D.E. Smailus, J.M. Stott, G.S. Yang, F. Plummer, A. Andonov, H. Artsob, N. Bastien, K. Bernard, T.F. Booth, D. Bowness, M. Czub, M. Drebolt, L. Fernando, R. Flick, M. Garbutt, M. Gray, A. Grolla, S. Jones, H. Feldmann, A. Meyers, A. Kabani, Y. Li, S. Normand, U. Stroher, G.A. Tipples, S. Tyler, R. Vogrig, D. Ward, B. Watson, R.C. Brunham, M. Krajden, M. Petric, D.M. Skowronski, C. Upton, R.L. Roper, The Genome sequence of the SARS-

- associated coronavirus, *Science* 300 (2003) 1399–1404.
- [24] Y.J. Ruan, C.L. Wei, A.L. Ee, V.B. Vega, H. Thoreau, S.T. Su, J.M. Chia, P. Ng, K.P. Chiu, L. Lim, T. Zhang, C.K. Peng, E.O. Lin, N.M. Lee, S.L. Yee, L.F. Ng, R.E. Chee, L.W. Stanton, P.M. Long, E.T. Liu, Comparative full-length genome sequence analysis of 14 SARS coronavirus isolates and common mutations associated with putative origins of infection, *Lancet* (London, England) 361 (2003) 1779–1785.
- [25] T.P. Sheahan, A.C. Sims, S.R. Leist, A. Schäfer, J. Won, A.J. Brown, S.A. Montgomery, A. Hogg, D. Babusis, M.O. Clarke, J.E. Spahn, L. Bauer, S. Sellers, D. Porter, J.Y. Feng, T. Cihlar, R. Jordan, M.R. Denison, R.S. Baric, Comparative therapeutic efficacy of remdesivir and combination lopinavir, ritonavir, and interferon beta against MERS-CoV, *Nat. Commun.* 11 (2020) 222.
- [26] B. Cao, Y. Wang, D. Wen, W. Liu, J. Wang, G. Fan, L. Ruan, B. Song, Y. Cai, M. Wei, X. Li, J. Xia, N. Chen, J. Xiang, T. Yu, T. Bai, X. Xie, L. Zhang, C. Li, Y. Yuan, H. Chen, H. Li, H. Huang, S. Tu, F. Gong, Y. Liu, Y. Wei, C. Dong, F. Zhou, X. Gu, J. Xu, Z. Liu, Y. Zhang, H. Li, L. Shang, K. Wang, K. Li, X. Zhou, X. Dong, Z. Qu, S. Lu, X. Hu, S. Ruan, S. Luo, J. Wu, L. Peng, F. Cheng, L. Pan, J. Zou, C. Jia, J. Wang, X. Liu, S. Wang, X. Wu, Q. Ge, J. He, H. Zhan, F. Qiu, L. Guo, C. Huang, T. Jaki, F.G. Hayden, P.W. Horby, D. Zhang, C. Wang, A trial of lopinavir-ritonavir in adults hospitalized with severe covid-19, *N. Engl. J. Med.* 382 (2020) 1787–1799.
- [27] J. Reina, Remdesivir, the antiviral hope against SARS-CoV-2, *Rev. Española Quimioter.* : Publ. Off. Soc. Española Quimioter. 33 (2020) 176–179.
- [28] M. Davies, V. Osborne, S. Lane, D. Roy, S. Dhanda, A. Evans, S. Shakir, Remdesivir in treatment of COVID-19: A systematic benefit–risk assessment, *Drug Saf.* (2020) 1–12. OnlineFirst.
- [29] Y. Chen, Q. Liu, D. Guo, Emerging coronaviruses: genome structure, replication, and pathogenesis, *J. Med. Virol.* 92 (2020) 418–423.
- [30] S. Hussain, J. Pan, Y. Chen, Y. Yang, J. Xu, Y. Peng, Y. Wu, Z. Li, Y. Zhu, P. Tien, D. Guo, Identification of novel subgenomic RNAs and noncanonical transcription initiation signals of severe acute respiratory syndrome coronavirus, *J. Virol.* 79 (2005) 5288–5295.
- [31] X. Liu, X. Wang, Potential inhibitors for 2019-nCoV coronavirus M protease from clinically approved medicines, *bioRxiv* (2020), <https://doi.org/10.1101/2020.01.29.924100>. Published online 29 January 2020.
- [32] H. Yang, M. Yang, Y. Ding, Y. Liu, Z. Lou, Z. Zhou, L. Sun, L. Mo, S. Ye, H. Pang, G.F. Gao, K. Anand, M. Bartlam, R. Hilgenfeld, Z. Rao, The crystal structures of severe acute respiratory syndrome virus main protease and its complex with an inhibitor, *Proc. Natl. Acad. Sci. U.S.A.* 100 (2003) 13190–13195.
- [33] U. Bacha, J. Barrila, A. Velazquez-Campoy, S.A. Leavitt, E. Freire, Identification of novel inhibitors of the SARS coronavirus main protease 3CLpro, *Biochemistry* 43 (2004) 4906–4912.
- [34] K. Anand, J. Ziebuhr, P. Wadhwani, J.R. Mesters, R. Hilgenfeld, Coronavirus main proteinase (3CLpro) structure: basis for design of anti-SARS drugs, *Science* 300 (2003) 1763–1767.
- [35] L. Lai, X. Han, H. Chen, P. Wei, C. Huang, S. Liu, K. Fan, L. Zhou, Z. Liu, J. Pei, Y. Liu, Quaternary structure, substrate selectivity and inhibitor design for SARS 3C-like proteinase, *Curr. Pharmaceut. Des.* 12 (2006) 4555–4564.
- [36] B. Xia, X. Kang, Activation and maturation of SARS-CoV main protease, *Protein Cell* 2 (2011) 282–290.
- [37] K. Fan, L. Ma, X. Han, H. Liang, P. Wei, Y. Liu, L. Lai, The substrate specificity of SARS coronavirus 3C-like proteinase, *Biochem. Biophys. Res. Commun.* 329 (2005) 934–940.
- [38] H. Yang, M. Bartlam, Z. Rao, Drug design targeting the main protease, the Achilles' heel of coronaviruses, *Curr. Pharmaceut. Des.* 12 (2006) 4573–4590.
- [39] M. Berry, B.C. Fielding, J. Gamieldien, Potential broad spectrum inhibitors of the coronavirus 3CLpro: a virtual screening and structure-based drug design study, *Viruses* 7 (2015) 6642–6660.
- [40] M.F. Hsu, C.J. Kuo, K.T. Chang, H.C. Chang, C.C. Chou, T.P. Ko, H.L. Shr, G.G. Chang, A.H. Wang, P.H. Liang, Mechanism of the maturation process of SARS-CoV 3CL protease, *J. Biol. Chem.* 280 (2005) 31257–31266.
- [41] K. Anand, G.J. Palm, J.R. Mesters, S.G. Siddell, J. Ziebuhr, R. Hilgenfeld, Structure of coronavirus main proteinase reveals combination of a chymotrypsin fold with an extra alpha-helical domain, *EMBO J.* 21 (2002) 3213–3224.
- [42] Y. Li, J. Zhang, N. Wang, H. Li, Y. Shi, G. Guo, K. Liu, H. Zeng, Q. Zou, Therapeutic drugs targeting 2019-nCoV main protease by high-throughput screening, *bioRxiv* (2020), <https://doi.org/10.1101/2020.01.28.922922>. Published online 28 January 2020.
- [43] R. Lu, X. Zhao, J. Li, P. Niu, B. Yang, H. Wu, W. Wang, H. Song, B. Huang, N. Zhu, Y. Bi, X. Ma, F. Zhan, L. Wang, T. Hu, H. Zhou, Z. Hu, W. Zhou, L. Zhao, J. Chen, Y. Meng, J. Wang, Y. Lin, J. Yuan, Z. Xie, J. Ma, W.J. Liu, D. Wang, W. Xu, E.C. Holmes, G.F. Gao, G. Wu, W. Chen, W. Shi, W. Tan, Genomic characterisation and epidemiology of 2019 novel coronavirus: implications for virus origins and receptor binding, *Lancet* (London, England) 395 (2020) 565–574.
- [44] F. Wu, S. Zhao, B. Yu, Y.M. Chen, W. Wang, Z.G. Song, Y. Hu, Z.W. Tao, J.H. Tian, Y.Y. Pei, M.L. Yuan, Y.L. Zhang, F.H. Dai, Y. Liu, Q.M. Wang, J.J. Zheng, L. Xu, E.C. Holmes, Y.Z. Zhang, A new coronavirus associated with human respiratory disease in China, *Nature* 579 (2020) 265–269.
- [45] P. Wei, K. Fan, H. Chen, L. Ma, C. Huang, L. Tan, D. Xi, C. Li, Y. Liu, A. Cao, L. Lai, The N-terminal octapeptide acts as a dimerization inhibitor of SARS coronavirus 3C-like proteinase, *Biochem. Biophys. Res. Commun.* 339 (2006) 865–872.
- [46] J. Jacobs, V. Grum-Tokars, Y. Zhou, M. Burlington, S.A. Saldanha, P. Chase, A. Eggler, E.S. Dawson, Y.M. Baez-Santos, S. Tomar, A.M. Mielech, S.C. Baker, C.W. Lindsley, P. Hodder, A. Mesecar, S.R. Stauffer, Discovery, synthesis, and structure-based optimization of a series of N-(tert-butyl)-2-(N-arylamo)-2-(pyridin-3-yl) acetamides (ML188) as potent noncovalent small molecule inhibitors of the severe acute respiratory syndrome coronavirus (SARS-CoV) 3CL protease, *J. Med. Chem.* 56 (2013) 534–546.
- [47] Y. Kim, S.R. Mandadapu, W.C. Groutas, K.O. Chang, Potent inhibition of feline coronaviruses with peptidyl compounds targeting coronavirus 3C-like protease, *Antivir. Res.* 97 (2013) 161–168.
- [48] A.K. Ghosh, K. Xi, K. Ratia, B.D. Santarsiero, W. Fu, B.H. Harcourt, P.A. Rota, S.C. Baker, M.E. Johnson, A.D. Mesecar, Design and synthesis of peptidomimetic severe acute respiratory syndrome chymotrypsin-like protease inhibitors, *J. Med. Chem.* 48 (2005) 6767–6771.
- [49] L. Zhu, S. George, M.F. Schmidt, S.I. Al-Gharabli, J. Rademann, R. Hilgenfeld, Peptide aldehyde inhibitors challenge the substrate specificity of the SARS-coronavirus main protease, *Antivir. Res.* 92 (2011) 204–212.
- [50] D.H. Goetz, Y. Choe, E. Hansell, Y.T. Chen, M. McDowell, C.B. Jonsson, W.R. Roush, J. McKerrow, C.S. Craik, Substrate specificity profiling and identification of a new class of inhibitor for the major protease of the SARS coronavirus, *Biochemistry* 46 (2007) 8744–8752.
- [51] H.Z. Zhang, H. Zhang, W. Kemnitzer, B. Tseng, J. Cinatl Jr., M. Michaelis, H.W. Doerr, S.X. Cai, Design and synthesis of dipeptidyl glutaminyl fluoromethyl ketones as potent severe acute respiratory syndrome coronavirus (SARS-CoV) inhibitors, *J. Med. Chem.* 49 (2006) 1198–1201.
- [52] M.O. Sydnes, Y. Hayashi, V.K. Sharma, T. Hamada, U. Bacha, J. Barrila, E. Freire, Y. Kiso, Synthesis of glutamic acid and glutamine peptides possessing a trifluoromethyl ketone group as SARS-CoV 3CL protease inhibitors, *Tetrahedron* 62 (2006) 8601–8609.
- [53] J.J. Shie, J.M. Fang, T.H. Kuo, C.J. Kuo, P.H. Liang, H.J. Huang, Y.T. Wu, J.T. Jan, Y.S. Cheng, C.H. Wong, Inhibition of the severe acute respiratory syndrome 3CL protease by peptidomimetic alpha,beta-unsaturated esters, *Bioorg. Med. Chem.* 13 (2005) 5240–5252.
- [54] A.K. Ghosh, K. Xi, V. Grum-Tokars, X. Xu, K. Ratia, W. Fu, K.V. Houser, S.C. Baker, M.E. Johnson, A.D. Mesecar, Structure-based design, synthesis, and biological evaluation of peptidomimetic SARS-CoV 3CLpro inhibitors, *Bioorg. Med. Chem. Lett* 17 (2007) 5876–5880.
- [55] S. Yang, S.J. Chen, M.F. Hsu, J.D. Wu, C.T. Tseng, Y.F. Liu, H.C. Chen, C.W. Kuo, C.S. Wu, L.W. Chang, W.C. Chen, S.Y. Liao, T.Y. Chang, H.H. Hung, H.L. Shr, C.Y. Liu, Y.A. Huang, L.Y. Chang, J.C. Hsu, C.J. Peters, A.H. Wang, M.C. Hsu, Synthesis, crystal structure, structure-activity relationships, and antiviral activity of a potent SARS coronavirus 3CL protease inhibitor, *J. Med. Chem.* 49 (2006) 4971–4980.
- [56] W. Dai, B. Zhang, X.-M. Jiang, H. Su, J. Li, Y. Zhao, X. Xie, Z. Jin, J. Peng, F. Liu, C. Li, Y. Li, F. Bai, H. Wang, X. Chen, X. Cen, S. Hu, X. Yang, J. Wang, X. Liu, G. Xiao, H. Jiang, Z. Rao, L.-K. Zhang, Y. Xu, H. Yang, H. Liu, Structure-based design, synthesis and biological evaluation of peptidomimetic aldehydes as a novel series of antiviral drug candidates targeting the SARS-CoV-2 main protease, *bioRxiv* (2020), <https://doi.org/10.1101/2020.03.25.996348>. Published online 25 March 2020.
- [57] Y.M. Shao, W.B. Yang, T.H. Kuo, K.C. Tsai, C.H. Lin, A.S. Yang, P.H. Liang, C.H. Wong, Design, synthesis, and evaluation of trifluoromethyl ketones as inhibitors of SARS-CoV 3CL protease, *Bioorg. Med. Chem.* 16 (2008) 4652–4660.
- [58] R.P. Jain, H.I. Pettersson, J. Zhang, K.D. Aull, P.D. Fortin, C. Huitema, L.D. Eltis, J.C. Parrish, M.N. James, D.S. Wishart, J.C. Vedera, Synthesis and evaluation of keto-glutamine analogues as potent inhibitors of severe acute respiratory syndrome 3CLpro, *J. Med. Chem.* 47 (2004) 6113–6116.
- [59] P. Thanigaimalai, S. Konno, T. Yamamoto, Y. Koiwai, A. Taguchi, K. Takayama, F. Yakushiji, K. Akaji, S.E. Chen, A. Naser-Tavakolian, A. Schön, E. Freire, Y. Hayashi, Development of potent dipeptide-type SARS-CoV 3CL protease inhibitors with novel P3 scaffolds: design, synthesis, biological evaluation, and docking studies, *Eur. J. Med. Chem.* 68 (2013) 372–384.
- [60] P. Thanigaimalai, S. Konno, T. Yamamoto, Y. Koiwai, A. Taguchi, K. Takayama, F. Yakushiji, K. Akaji, Y. Kiso, Y. Kawasaki, S.E. Chen, A. Naser-Tavakolian, A. Schön, E. Freire, Y. Hayashi, Design, synthesis, and biological evaluation of novel dipeptide-type SARS-CoV 3CL protease inhibitors: structure-activity relationship study, *Eur. J. Med. Chem.* 65 (2013) 436–447.
- [61] L. Zhang, D. Lin, Y. Kusov, Y. Nian, Q. Ma, J. Wang, A. von Brunn, P. Leyssen, K. Lanko, J. Neyts, A. de Wilde, E.J. Snijder, H. Liu, R. Hilgenfeld, α -Ketoamides as broad-spectrum inhibitors of coronavirus and enterovirus replication: structure-based design, synthesis, and activity assessment, *J. Med. Chem.* 63 (2020) 4562–4578.
- [62] W. Dai, B. Zhang, X.-M. Jiang, H. Su, J. Li, Y. Zhao, X. Xie, Z. Jin, J. Peng, F. Liu, C. Li, Y. Li, F. Bai, H. Wang, X. Chen, X. Cen, S. Hu, X. Yang, J. Wang, X. Liu, G. Xiao, H. Jiang, Z. Rao, L.-K. Zhang, Y. Xu, H. Yang, H. Liu, Structure-based design, synthesis and biological evaluation of peptidomimetic aldehydes as a novel series of antiviral drug candidates targeting the SARS-CoV-2 main protease, *bioRxiv* (2020), 2020.03.25.996348.
- [63] L. Zhang, D. Lin, X. Sun, U. Curth, C. Drosten, L. Sauerhering, S. Becker, K. Rox, R. Hilgenfeld, Crystal structure of SARS-CoV-2 main protease provides a basis for design of improved α -ketoamide inhibitors, *Science* (2020).
- [64] T. Pillaiy, M. Manickam, V. Namasivayam, Y. Hayashi, S. Jung, An overview of severe acute respiratory syndrome–coronavirus (SARS-CoV) 3CL protease inhibitors: peptidomimetics and small molecule chemotherapy, *J. Med.*

- Chem. 59 (2016) 6595–6628.
- [65] Y. Shimamoto, Y. Hattori, K. Kobayashi, K. Teruya, A. Sanjoh, A. Nakagawa, E. Yamashita, K. Akaji, Fused-ring structure of decahydroisoquinolin as a novel scaffold for SARS 3CL protease inhibitors, *Bioorg. Med. Chem.* 23 (2015) 876–890.
- [66] S. Yoshizawa, Y. Hattori, K. Kobayashi, K. Akaji, Evaluation of an octahydroisochromene scaffold used as a novel SARS 3CL protease inhibitor, *Bioorg. Med. Chem.* 28 (2020) 115273.
- [67] K. Ohnishi, Y. Hattori, K. Kobayashi, K. Akaji, Evaluation of a non-prime site substituent and warheads combined with a decahydroisoquinolin scaffold as a SARS 3CL protease inhibitor, *Bioorg. Med. Chem.* 27 (2019) 425–435.
- [68] M. Turlington, A. Chun, S. Tomar, A. Eggler, V. Grum-Tokars, J. Jacobs, J.S. Daniels, E. Dawson, A. Saldanha, P. Chase, Y.M. Baez-Santos, C.W. Lindsley, P. Hodder, A.D. Mesecar, S.R. Stauffer, Discovery of N-(benzo[1,2,3]triazol-1-yl)-N-(benzyl)acetamido)phenyl carboxamides as severe acute respiratory syndrome coronavirus (SARS-CoV) 3CLpro inhibitors: identification of ML300 and noncovalent nanomolar inhibitors with an induced-fit binding, *Bioorg. Med. Chem. Lett.* 23 (2013) 6172–6177.
- [69] K. Karypidou, S.R. Ribone, M.A. Quevedo, L. Persoons, C. Pannecouque, C. Helsen, F. Claessens, W. Dehaen, Synthesis, biological evaluation and molecular modeling of a novel series of fused 1,2,3-triazoles as potential anti-coronavirus agents, *Bioorg. Med. Chem. Lett.* 28 (2018) 3472–3476.
- [70] A.C.G. Kankanamalage, Y. Kim, V.C. Damalanka, A.D. Rathnayake, A.R. Fehr, N. Mehzabeen, K.P. Battaile, S. Lovell, G.H. Lushington, S. Perlman, K.O. Chang, W.C. Groutas, Structure-guided design of potent and permeable inhibitors of MERS coronavirus 3CL protease that utilize a piperidine moiety as a novel design element, *Eur. J. Med. Chem.* 150 (2018) 334–346.
- [71] L. Wang, B. Bao, G. Song, C. Chen, X. Zhang, W. Lu, Z. Wang, Y. Cai, S. Li, S. Fu, Discovery of unsymmetrical aromatic disulfides as novel inhibitors of SARS-CoV main protease: chemical synthesis, biological evaluation, molecular docking and 3D-QSAR study, *Eur. J. Med. Chem.* 137 (2017) 450–461.
- [72] H. Konno, T. Onuma, I. Nitani, M. Wakabayashi, S. Yano, K. Teruya, K. Akaji, Synthesis and evaluation of phenylisoserine derivatives for the SARS-CoV 3CL protease inhibitor, *Bioorg. Med. Chem. Lett.* 27 (2017) 2746–2751.
- [73] H. Konno, M. Wakabayashi, D. Takanuma, Y. Saito, K. Akaji, Design and synthesis of a series of serine derivatives as small molecule inhibitors of the SARS coronavirus 3CL protease, *Bioorg. Med. Chem.* 24 (2016) 1241–1254.
- [74] K. Akaji, H. Konno, H. Mitsui, K. Teruya, Y. Shimamoto, Y. Hattori, T. Ozaki, M. Kusunoki, A. Sanjoh, Structure-based design, synthesis, and evaluation of peptide-mimetic SARS 3CL protease inhibitors, *J. Med. Chem.* 54 (2011) 7962–7973.
- [75] Q. Yang, L. Chen, X. He, Z. Gao, X. Shen, D. Bai, Design and synthesis of cinanserin analogs as severe acute respiratory syndrome coronavirus 3CL protease inhibitors, *Chem. Pharmaceut. Bull.* 56 (2008) 1400–1405.
- [76] R. Ramajayam, K. Tan, H. Liu, P. Liang, Synthesis and evaluation of pyrazolone compounds as SARS-coronavirus 3C-like protease inhibitors, *Bioorg. Med. Chem.* 18 (2010) 7849–7854.
- [77] V. Kumar, K. Tan, Y. Wang, S. Lin, P. Liang, Identification, synthesis and evaluation of SARS-CoV and MERS-CoV 3C-like protease inhibitors, *Bioorg. Med. Chem.* 24 (2016) 3035–3042.
- [78] R. Ramajayam, K. Tan, H. Liu, P. Liang, Synthesis, docking studies, and evaluation of pyrimidines as inhibitors of SARS-CoV 3CL protease, *Bioorg. Med. Chem. Lett.* 20 (2010) 3569–3572.
- [79] T.T.H. Nguyen, H. Woo, H. Kang, V.D. Nguyen, Y. Kim, D.W. Kim, S. Ahn, Y. Xia, D. Kim, Flavonoid-mediated inhibition of SARS coronavirus 3C-like protease expressed in *Pichia pastoris*, *Biotechnol. Lett.* 34 (2012) 831–838.
- [80] Y.B. Ryu, H.J. Jeong, J.H. Kim, Y. Kim, J. Park, D. Kim, T.T.H. Naguyen, S. Park, J.S. Chang, K.H. Park, Biflavonoids from *Torreya nucifera* displaying SARS-CoV 3CLpro inhibition, *Bioorg. Med. Chem.* 18 (2010) 7940–7947.
- [81] J. Park, J. Ko, D.W. Kim, Y.M. Kim, H. Kwon, H.J. Jeong, C.Y. Kim, K.H. Park, W.S. Lee, Y.B. Ryu, Chalcones isolated from *Angelica keiskei* inhibit cysteine proteases of SARS-CoV, *J. Enzym. Inhib. Med. Chem.* 31 (2016) 23–30.
- [82] H. Guo, Isatin derivatives and their anti-bacterial activities, *Eur. J. Med. Chem.* 164 (2019) 678–688.
- [83] A.A. Farag, Synthesis and antimicrobial activity of 5-(morpholinosulfonyl) isatin derivatives incorporating a thiazole moiety, *Drug Res.* 65 (2015) 373–379.
- [84] A. Jarrahpour, J. Sheikh, I. Mounsi, H. Juneja, T. Hadda, Computational evaluation and experimental in vitro antibacterial, antifungal and antiviral activity of bis-Schiff bases of isatin and its derivatives, *Med. Chem. Res.* 22 (2012) 1203–1211.
- [85] R. Meleddu, S. Distinto, A. Corona, E. Tramontano, G. Bianco, C. Melis, F. Cottiglia, E. Maccioni, Isatin thiazoline hybrids as dual inhibitors of HIV-1 reverse transcriptase, *J. Enzym. Inhib. Med. Chem.* 32 (2017) 130–136.
- [86] A. Corona, R. Meleddu, F. Esposito, S. Distinto, G. Bianco, T. Masaoka, E. Maccioni, L. Menéndez-Arias, S. Alcaro, S.F. Le Grice, E. Tramontano, Ribonuclease H/DNA polymerase HIV-1 reverse transcriptase dual inhibitor: mechanistic studies on the allosteric mode of action of isatin-based compound RMNC6, *PLoS One* 11 (2016), e0147225.
- [87] P. Selvam, N. Murgesh, M. Chandramohan, E. De Clercq, E. Keyaerts, L. Vijgen, P. Maes, J. Neyts, M.V. Ranst, Vitro antiviral activity of some novel isatin derivatives against HCV and SARS-CoV viruses, *Indian J. Pharmaceut. Sci.* 70 (2008) 91–94.
- [88] F. Gao, H. Yang, T. Lu, Z. Chen, L. Ma, Z. Xu, P. Schaffer, G. Lu, Design, synthesis and anti-mycobacterial activity evaluation of benzofuran-isatin hybrids, *Eur. J. Med. Chem.* 159 (2018) 277–281.
- [89] S.B. Kumar, M. Ravinder, G. Kishore, V. Jayathirtha Rao, P. Yogeeshwari, D. Sriram, Synthesis, antitubercular and anticancer activity of new Baylis-Hillman adduct-derived N-cinnamyl-substituted isatin derivatives, *Med. Chem. Res. : Int. J. Rapid Commun. Des. Mech. Action Biol. Active Agents* 23 (2014) 1934–1940.
- [90] L.R. Chen, Y.C. Wang, Y.W. Lin, S.Y. Chou, S.F. Chen, L.T. Liu, Y.T. Wu, C.J. Kuo, T.S. Chen, S.H. Juang, Synthesis and evaluation of isatin derivatives as effective SARS coronavirus 3CL protease inhibitors, *Bioorg. Med. Chem. Lett.* 15 (2005) 3058–3062.
- [91] W. Liu, H.-M. Zhu, G.-J. Niu, E.-Z. Shi, J. Chen, B. Sun, W.-Q. Chen, H.-G. Zhou, C. Yang, Synthesis, modification and docking studies of 5-sulfonyl isatin derivatives as SARS-CoV 3C-like protease inhibitors, *Bioorg. Med. Chem. Lett.* 22 (2013) 292–302.
- [92] J. Park, J.H. Kim, Y. Kim, H.J. Jeong, D.W. Kim, K.H. Park, H. Kwon, S. Park, W.S. Lee, Y.B. Ryu, Tanshinones as selective and slow-binding inhibitors for SARS-CoV cysteine proteases, *Bioorg. Med. Chem.* 20 (2012) 5928–5935.
- [93] Y.B. Ryu, S. Park, Y. Kim, J. Lee, W.D. Seo, J.S. Chang, K.H. Park, M. Rho, W.S. Lee, SARS-CoV 3CLpro inhibitory effects of quinone-methide triterpenes from *Tripterygium regelii*, *Bioorg. Med. Chem. Lett.* 20 (2010) 1873–1876.
- [94] L. Zhou, Y. Liu, W. Zhang, P. Wei, C. Huang, J. Pei, Y. Yuan, L. Lai, Isatin compounds as noncovalent SARS coronavirus 3C-like protease inhibitors, *J. Med. Chem.* 49 (2006) 3440–3443.
- [95] D. Basu, A. Richters, D. Rauh, Structure-based design and synthesis of covalent-reversible inhibitors to overcome drug resistance in EGFR, *Bioorg. Med. Chem.* 23 (2016) 2767–2780.
- [96] I.M. Serafimova, M.A. Pufall, S. Krishnan, K. Duda, M.S. Cohen, R.L. Maglathlin, J.M. McFarland, R.M. Miller, M. Frödin, J. Taunton, Reversible targeting of noncatalytic cysteines with chemically tuned electrophiles, *Nat. Chem. Biol.* 8 (2012) 471–476.
- [97] R.M. Miller, V.O. Paavilainen, S. Krishnan, I.M. Serafimova, J. Taunton, Electrophilic fragment-based design of reversible covalent kinase inhibitors, *J. Am. Chem. Soc.* 135 (2013) 5298–5301.
- [98] S. Krishnan, R.M. Miller, B. Tian, R.D. Mullins, M.P. Jacobson, J. Taunton, Design of reversible, cysteine-targeted Michael acceptors guided by kinetic and computational analysis, *J. Am. Chem. Soc.* 136 (2014) 12624–12630.
- [99] A.C. Lai, C.M. Crews, Induced protein degradation: an emerging drug discovery paradigm, *Nat. Rev. Drug Discov.* 16 (2017) 101–114.
- [100] M. Schapira, M.F. Calabrese, A.N. Bullock, C.M. Crews, Targeted protein degradation: expanding the toolbox, *Nature reviews, Drug Discov.* 18 (2019) 949–963.
- [101] X. Sun, H. Gao, Y. Yang, M. He, Y. Wu, Y. Song, Y. Tong, Y. Rao, PROTACs: great opportunities for academia and industry, *Signal Transduct. Target Ther.* 4 (2019) 64.
- [102] P.P. Chamberlain, A. Lopez-Girona, K. Miller, G. Carmel, B. Pagarigan, B. Chie-Leon, E. Rychak, L.G. Corral, Y.J. Ren, M. Wang, M. Riley, S.L. Delker, T. Ito, H. Ando, T. Mori, Y. Hirano, H. Handa, T. Hakoshima, T.O. Daniel, B.E. Cathers, Structure of the human Cereblon-DDB1-lenalidomide complex reveals basis for responsiveness to thalidomide analogs, *Nat. Struct. Mol. Biol.* 21 (2014) 803–809.
- [103] E.S. Fischer, K. Böhm, J.R. Lydeard, H. Yang, M.B. Stadler, S. Cavadi, J. Nagel, F. Serluca, V. Acker, G.M. Lingaraju, R.B. Tichkule, M. Schebesta, W.C. Forrester, M. Schirle, U. Hassiepen, J. Ottl, M. Hild, R.E. Beckwith, J.W. Harper, J.L. Jenkins, N.H. Thomä, Structure of the DDB1-CRBN E3 ubiquitin ligase in complex with thalidomide, *Nature* 512 (2014) 49–53.
- [104] B.E. Smith, S.L. Wang, S. Jaime-Figueroa, A. Harbin, J. Wang, B.D. Hamman, C.M. Crews, Differential PROTAC substrate specificity dictated by orientation recruited E3 ligase, *Nat. Commun.* 10 (2019) 131.
- [105] A. Rodriguez-Gonzalez, K. Cyrus, M. Salcius, K. Kim, C.M. Crews, R.J. Deshaies, K.M. Sakamoto, Targeting steroid hormone receptors for ubiquitination and degradation in breast and prostate cancer, *Oncogene* 27 (2008) 7201–7211.
- [106] M.S. Gadd, A. Testa, X. Lucas, K.H. Chan, W. Chen, D.J. Lamont, M. Zengerle, A. Ciulli, Structural basis of PROTAC cooperative recognition for selective protein degradation, *Nat. Chem. Biol.* 13 (2017) 514–521.
- [107] M. de Wispelaere, G. Du, K. Donovan, T. Zhang, N. Eleuteri, J. Yuan, J. Kalabathula, R. Nowak, E. Fischer, N. Gray, P. Yang, Small molecule degraders of the hepatitis C virus protease reduce susceptibility to resistance mutations, *Nat. Commun.* 10 (2019) 1–11.